Electronic Supplementary Material (ESI) for CrystEngComm.
This journal is © The Royal Society of Chemistry 2014

SUPPORTING INFORMATION

Ex-situ and *in-situ* monitoring of the syntheses of thermochromic Schiff bases

Marija Zbačnik* and Branko Kaitner

*Laboratory of General and Inorganic Chemistry, Department of Chemistry, Faculty of Science,
University of Zagreb, Horvatovac 102a, HR-10002 Zagreb, Croatia*

Email: mzbacnik@chem.pmf.hr
Fax: +385 1 4606 341
Tel: +385 1 4606 379

Table of Contents

Experimental details

Materials

The starting materials, salicylaldehyde was purchased from Merck, *o*-vanillin from Acros Organics, *o*-hydroxysalicylaldehyde, *p*-hydroxysalicylaldehyde and *α*-aminodiphenylmethane from Aldrich, 2-aminonaphthalene from Carlo Erba, 1-aminonaphthalene, acetone (**ace**), acetonitrile (**acn**), methanol (**MeOH**), ethanol (**EtOH**), chloroform (**chl**) and tetrahydrofuran (**thf**) from Kemika and used as purchased.

Synthesis

General procedure

The syntheses of **1-7** were performed by grinding equimolar quantities of aldehyde and amine (1 mmol : 1 mmol) in an agate mortar. The powder products were at that point qualitatively identified by PXRD to decide should the synthesis be repeated in different conditions *e.g.* liquid assisted grinding and/or ball milling.

Synthesis of **1**

Equimolar quantities of **sal** (0.122 g, 1 mmol) and **2an** (0.143 g, 1 mmol) were ground in an agate mortar at 25 °C for 4.5 min.

Synthesis of **2**

Equimolar quantities of ***o*-van** (0.153 g, 1 mmol) and **2an** (0.143 g, 1 mmol) were ground in an agate mortar at 25 °C for 5 min. The PXRD revealed that the used procedure is not efficient enough since there are traces of reactants in the powder product. Therefore, the synthesis of **2** was repeated in a Retsch MM200 grinder mill operating at 25 Hz frequency for 30 minutes. The reactants and two stainless steel grinding balls 7 mm in diameter were put in a stainless steel jar of 10 mL volume.

Synthesis of **3a**

Equimolar quantities of ***o*-van** (0.153 g, 1 mmol) and **1an** (0.143 g, 1 mmol) were ground in an agate mortar at 25 °C for 15 min. The synthesis was also repeated by solution-based synthesis to verify the role of acetonitrile in the formation of **3a**.

Synthesis of **3b**

Compound **3b** was obtained by solution-based synthesis. Equimolar quantities ***o*-van** (0.153 g, 1 mmol) and **1an** (0.143 g, 1 mmol) were dissolved in methanol (5 mL and 5 mL, respectively). The solutions were mixed and the resulting mixture left at room temperature. Red precipitate began to appear after few minutes.

Synthesis of **4**

Equimolar quantities of ***o*-OHsal** (0.135 g, 1 mmol) and **1an** (0.143 g, 1 mmol) were ground in an agate mortar at 25 °C for 4 min.

Synthesis of **5**

Equimolar quantities of ***p*-OHsal** (0.135 g, 1 mmol) and **1an** (0.143 g, 1 mmol) were ground in an agate mortar at 25 °C for 10 min. PXRD revealed traces of reactants in the powder product. Therefore, the synthesis of **5** was repeated in a Retsch MM200 grinder mill operating at 25 Hz frequency for 30 minutes. The reactants and two stainless steel grinding balls 7 mm in diameter were put in a stainless steel jar of 10 mL volume. Once more, the PXRD pattern revealed traces of reactants. Thus, the synthesis was repeated in the agate mortar at 25 °C with the same amount of reactants and 20 μL of acetonitrile for 4 min.

Synthesis of **6**

Equimolar quantities of **sal** (0.122 g, 1 mmol) and **adpm** (0.183 g, 1 mmol) were ground in an agate mortar at 25 °C for 2.5 min.

Synthesis of **7**

Equimolar quantities of ***o*-van** (0.153 g, 1 mmol) and **adpm** (0.183 g, 1 mmol) were ground in an agate mortar at 25 °C for 10 min. The reaction mixture remained as a liquid until 20 μL of ethanol was added into it. The grinding process lasted 10 minutes in overall.

The syntheses were doubled to check the reproducibility.

Thermal analysis

The measurements were performed on a Mettler Toledo TGA/SDTA and DSC823^e module in sealed aluminium pans (40 μL), heated in flowing nitrogen (200 mL min^{-1}) at a rate of 10 °C min^{-1}. The data collection and analysis was performed using the program package STAR^e Software 9.01. [5].

FT-IR spectroscopy

Infrared spectra were recorded on an EQUINOX 55 FTIR spectrophotometer using the KBr pellet method. The data collection and analysis was performed using the program package OPUS 4.0. [6] Table S8 comprises data for the characteristic stretching bands for **2**, **3a**, **5** and **7**.

NMR spectroscopy

^{1}H- and ^{13}C-NMR spectra were recorded in DMSO on Varian Gemini XL300 spectrometer. The spectral analysis was performed using the program package SpinWorks 3 [7]. Characteristic signals for **2**, **3a**, **5** and **7** found in the ^{1}H- and ^{13}C-NMR spectra are listed in Table S9 and S10, respectively.

Single crystal X-Ray diffraction experiments

Crystal and molecular structures of **1–7** at 298 and 110 K were determined using single crystal X-ray diffraction. Diffraction measurements were made on an Oxford Diffraction Xcalibur Kappa CCD X-ray diffractometer with graphite-monochromated MoK_α (λ = 0.71073 Å) radiation [8]. The data sets were collected using the ω scan mode over the 2θ range up to 54°. The structures were solved by direct methods and refined using the SHELXS and SHELXL programs, respectively [9]. The structural refinement was performed on F^2 using all data. The hydrogen atoms not involved in hydrogen bonding were placed in calculated positions and treated as riding on their parent atoms [C–H = 0.93 Å and $U_{\mathrm{iso}}(\mathrm{H}) = 1.2\ U_{\mathrm{eq}}(\mathrm{C})$; C–H = 0.97 Å and $U_{\mathrm{iso}}(\mathrm{H}) = 1.2\ U_{\mathrm{eq}}(\mathrm{C})$] while the others were located from the electron difference map. All calculations were performed using the WinGX crystallographic suite of programs [10]. The data concerning the results of the crystallographic experiments of until now unreported structures are listed in Table S2 to S8. Further details are available from the Cambridge Crystallographic Centre [11]. Molecular structures of compounds are presented by ORTEP-3 [12] and their packing diagrams were prepared using Mercury [13].

Powder X-Ray diffraction experiments

The powder X-ray diffraction (PXRD) experiments were performed on a PHILIPS PW 1840 X-ray diffractometer with $\mathrm{Cu}K_{\alpha 1}$ (1.54056 Å) radiation at 40 mA and 40 kV. The scattered intensities were measured with a scintillation counter. The angular range (2θ) was from 5 to 45° with steps of 0.02°, and the measuring time was 0.5 s per step. The data collection and analysis were performed using the program package *Philips X'Pert* [14,15,16].

Table S1. The IUPAC names for **1**–**7**.

Compound	IUPAC name
1	2-(Naphthalen-2-yliminomethyl)-phenol
2	2-Methoxy-6-(Naphthalene-2-yliminomethyl)-phenol
3	2-Methoxy-6-(Naphthalene-1-yliminomethyl)-phenol
4	2-Hydroxy-6-(Naphthalene-1-ylaminomethylene)-cyclohexa-2,4-dienone
5	2-(Naphthalen-1-yliminomethyl)-benzene-1,4-diol
6	2-(Benzhydrylimino-methyl)-phenol
7	2-(Benzhydrylimino-methyl)-6-methoxy-phenol

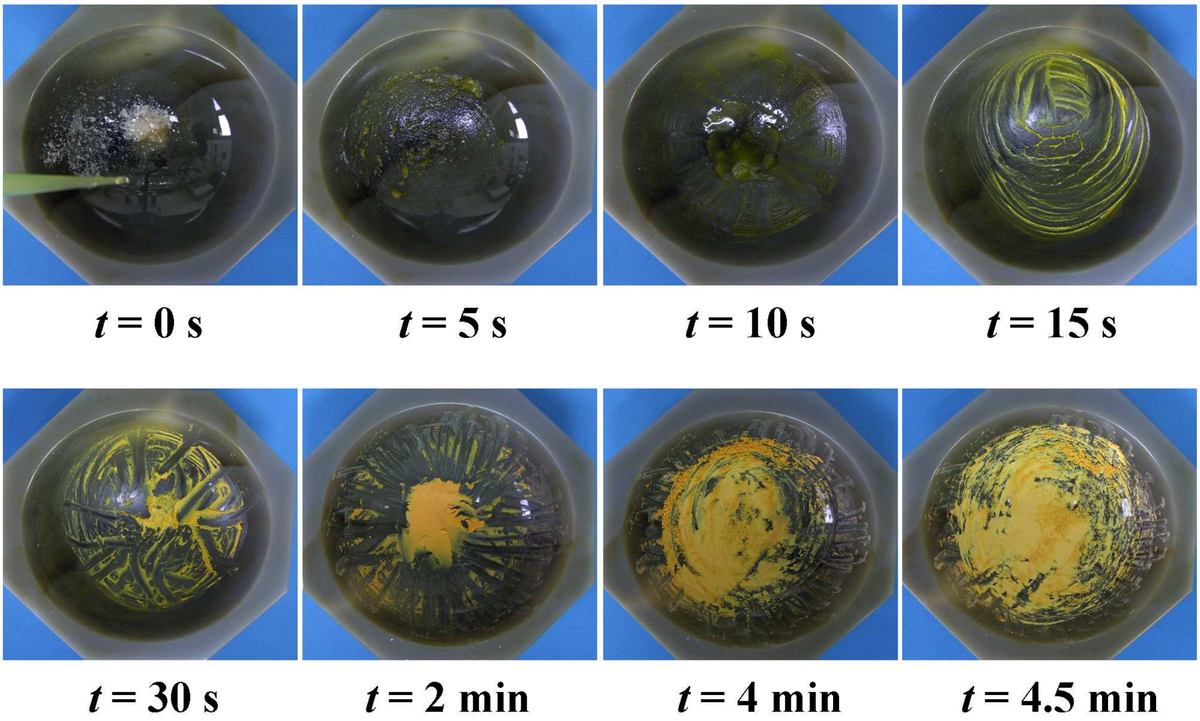

***t* = 0 s** ***t* = 5 s** ***t* = 10 s** ***t* = 15 s**

***t* = 30 s** ***t* = 2 min** ***t* = 4 min** ***t* = 4.5 min**

Figure S1. Synthesis of **1** in the agate mortar.

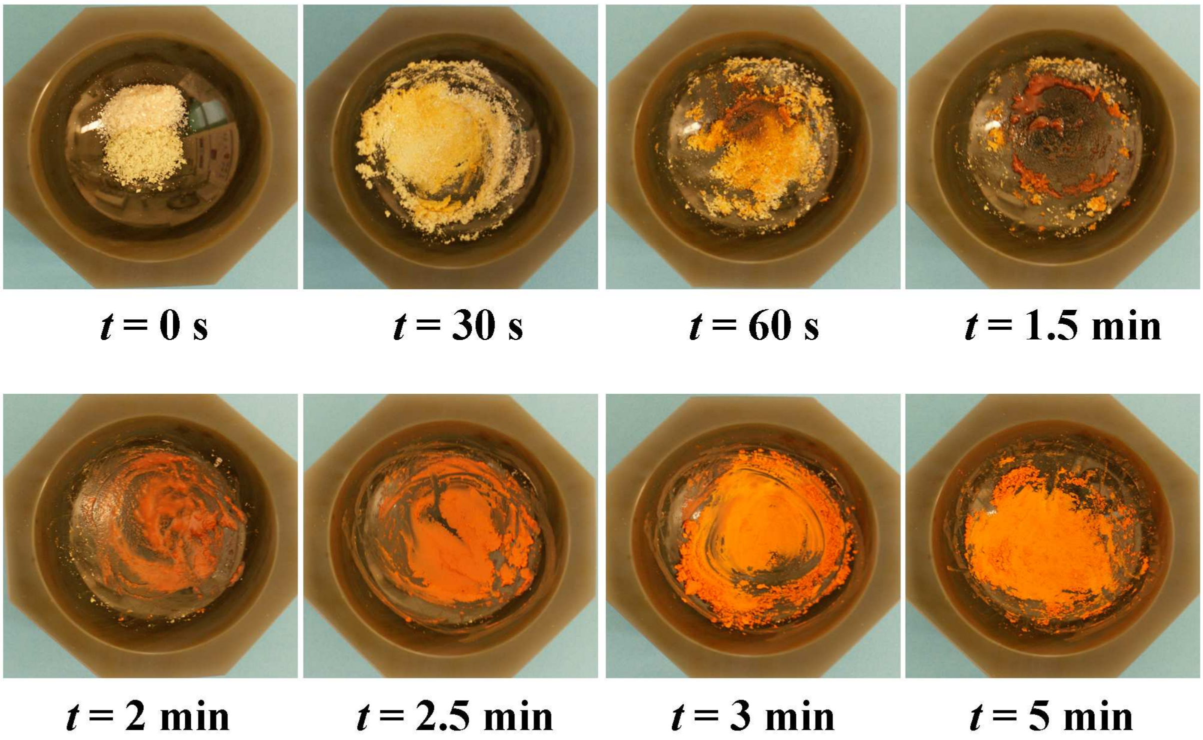

Figure S2. Synthesis of **2** in the agate mortar.

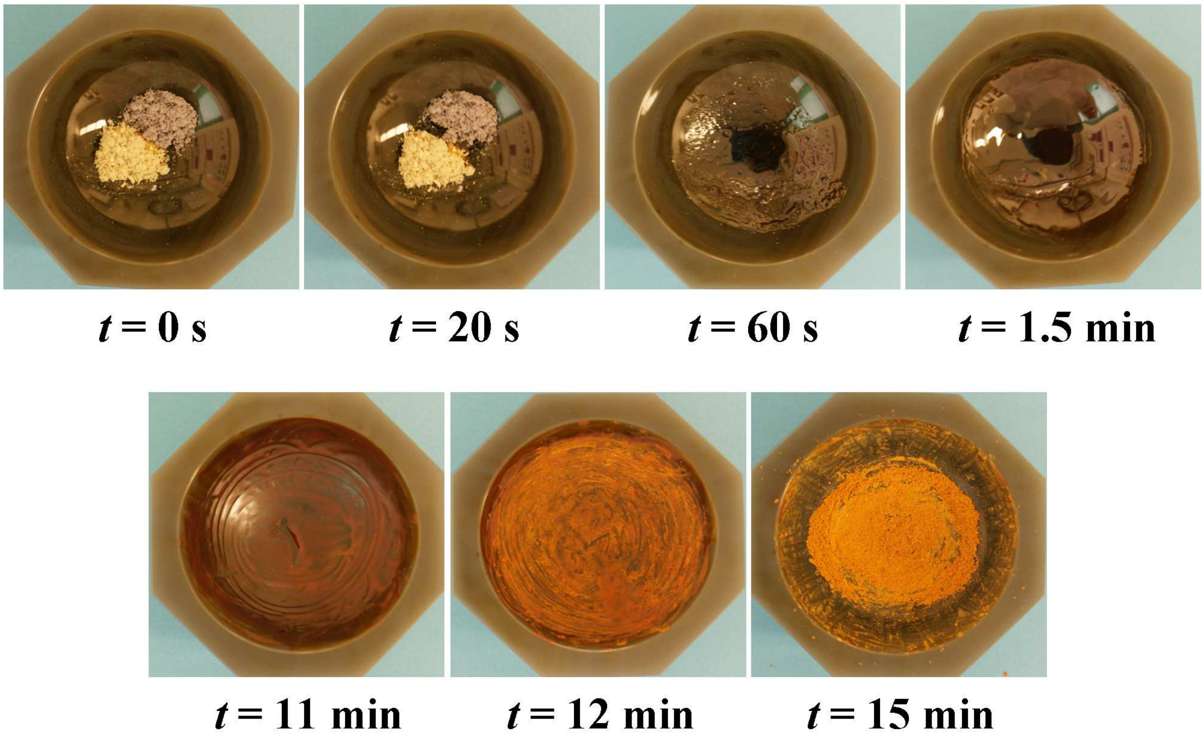

Figure S3. Synthesis of **3a** in the agate mortar.

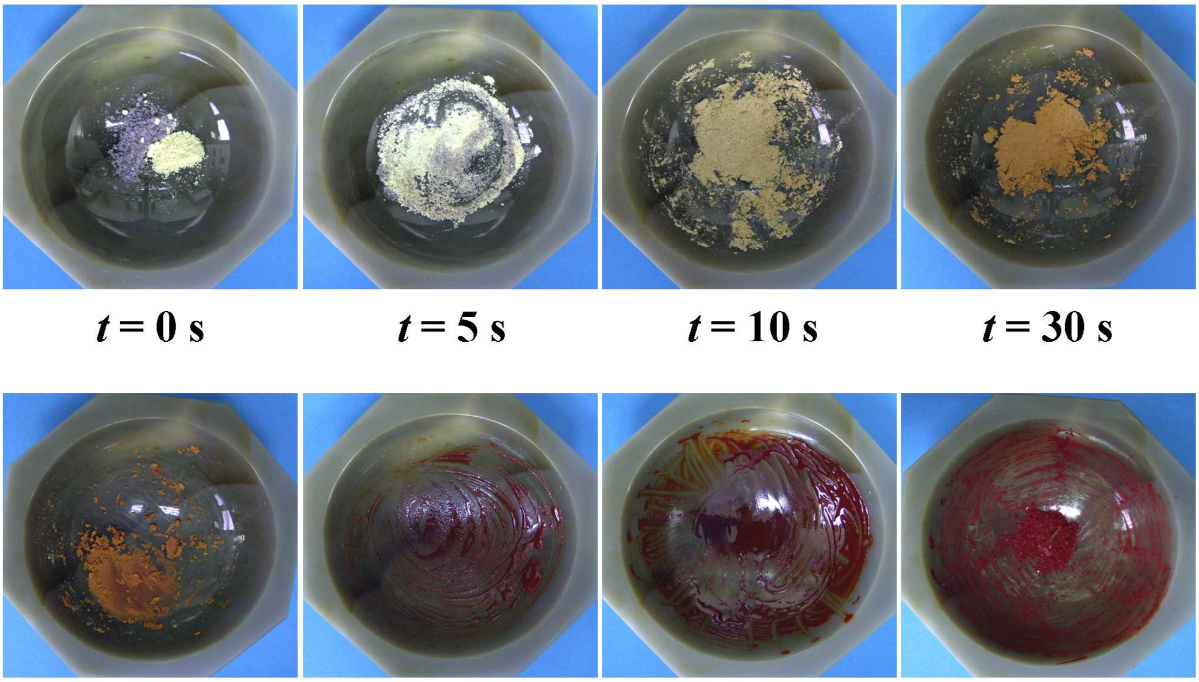

t = 0 s   *t* = 5 s   *t* = 10 s   *t* = 30 s

t = 60 s   *t* = 2 min   *t* = 3 min   *t* = 4 min

Figure S4. Synthesis of **4** in the agate mortar.

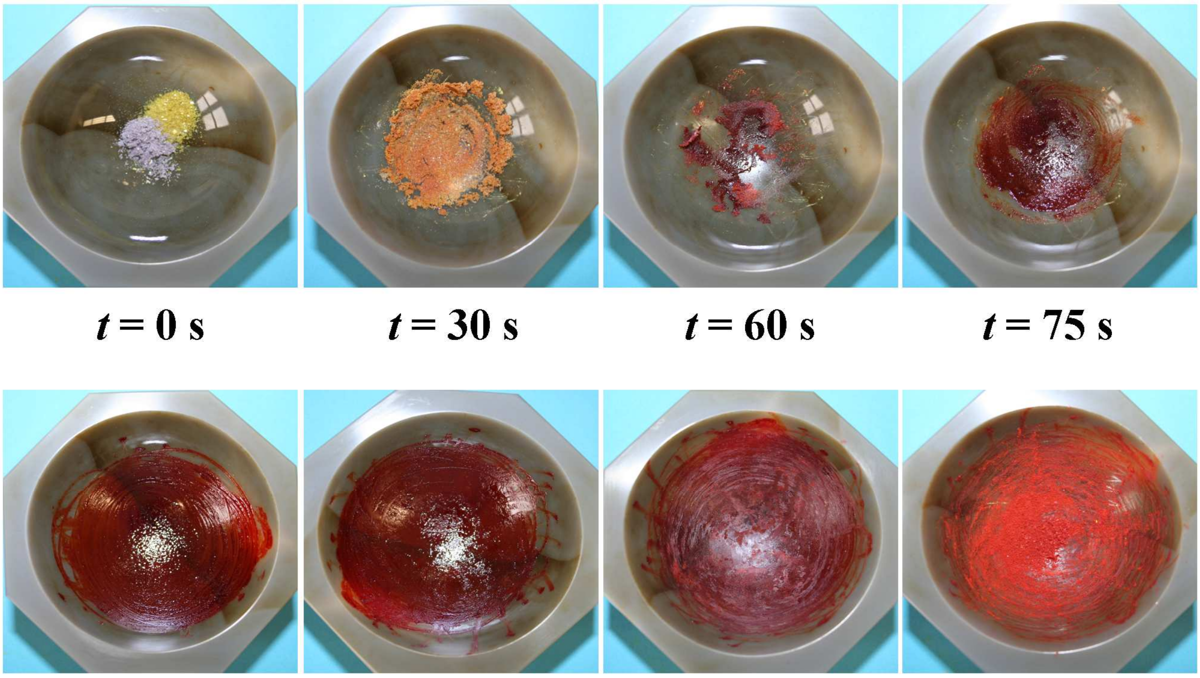

t = 0 s   *t* = 30 s   *t* = 60 s   *t* = 75 s

t = 2.5 min   *t* = 3.5 min   *t* = 5 min   *t* = 10 min

Figure S5. Synthesis of **5** in the agate mortar.

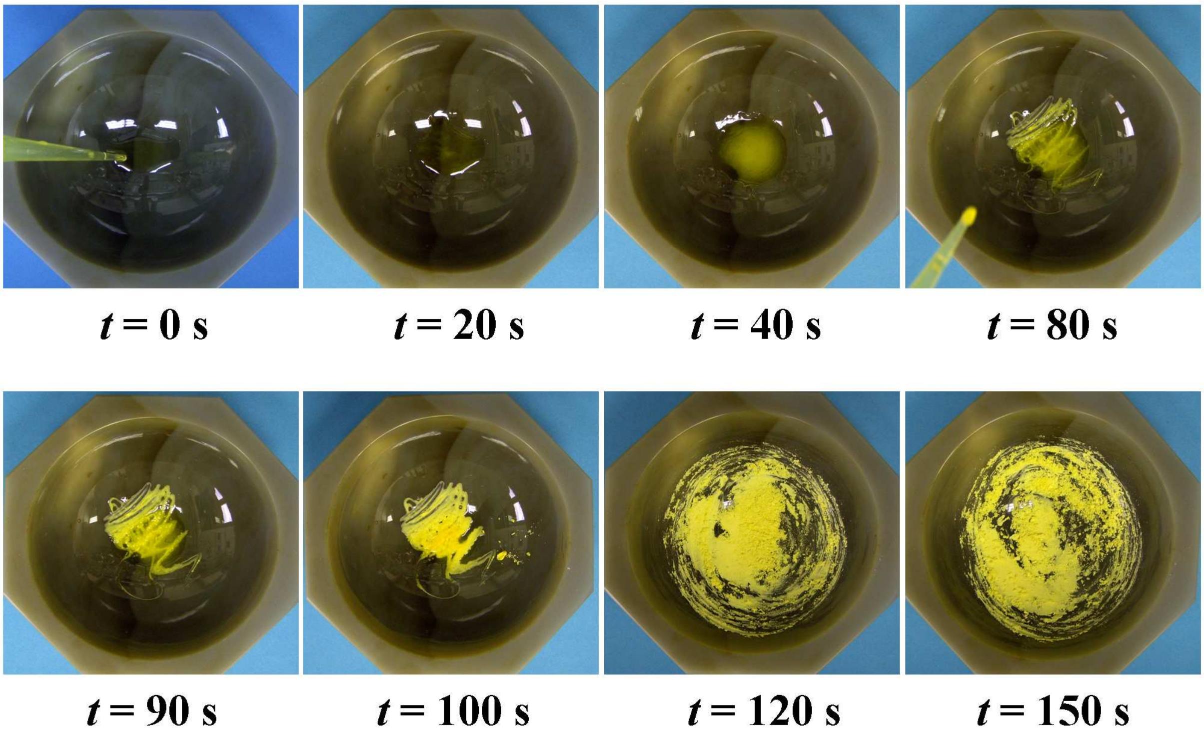

Figure S6. Synthesis of **6** in the agate mortar.

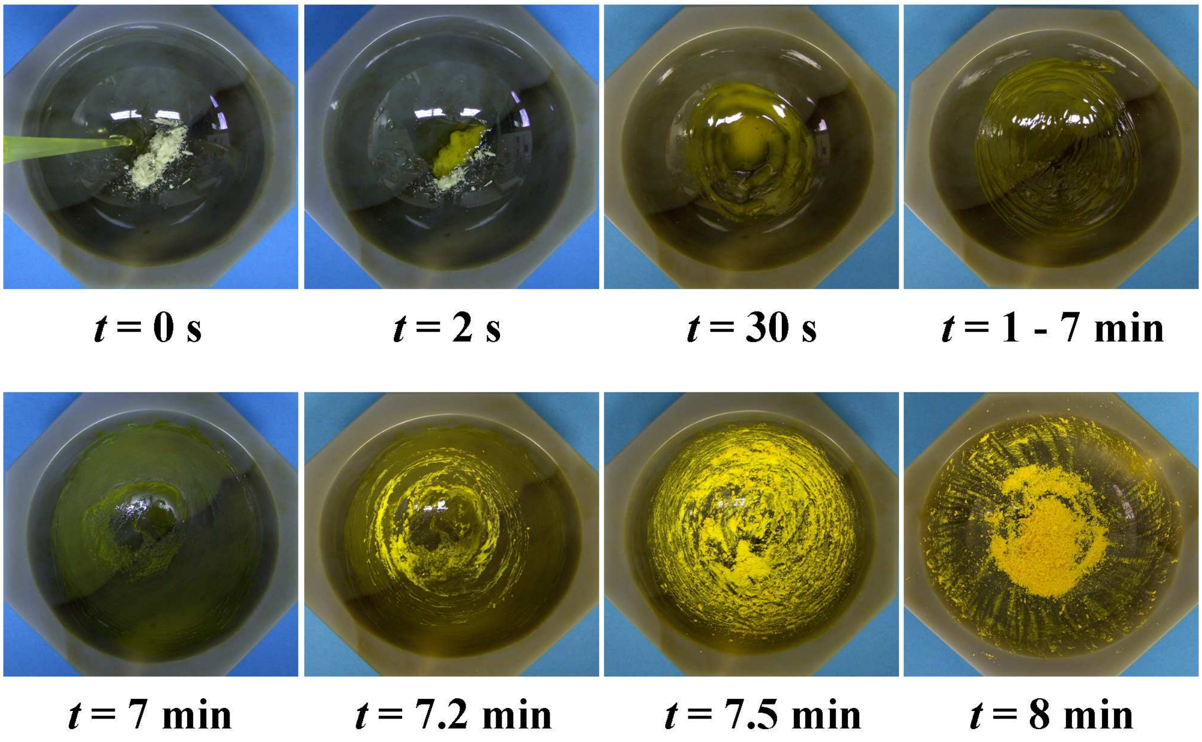

Figure S7. Synthesis of **7** in the agate mortar.

Table S2. General and crystallographic data for **1** at 110 K.

Structural formula	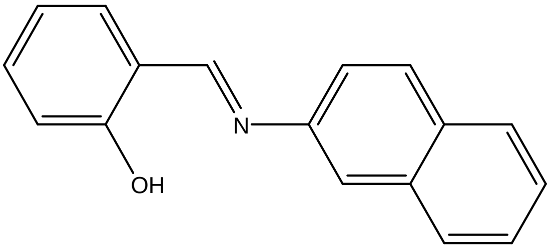
Molecular formula	$C_{17}H_{13}NO$
M_r	247.29
Crystal system	Orthorhombic
Space group	$P\,ca2_1$
Crystal data:	
a / Å	13.5629(4)
b / Å	5.8307(2)
c / Å	15.6428(5)
V / Å^3	1237.05(7)
Z	4
D_{calc} / g cm^{-3}	1.328
λ(MoK_α) / Å	0.71073
μ / mm^{-1}	0.083
Crystal size / mm^3	0.88 x 0.76 x 0.56
$F(000)$	520
Refl. collected/unique	5257 / 2621
Data/Restraints/Parameters	173
$\Delta\rho_{\max}$, $\Delta\rho_{\min}$ / e Å^{-3}	0.180; –0.166
$R[F^2 \geq 2\sigma(F^2)]$	0.0319
$wR(F^2)$	0.0816
Goodness-of-fit, S	0.988

Table S3. General and crystallographic data for **2** at 298 and 110 K.

Structural formula	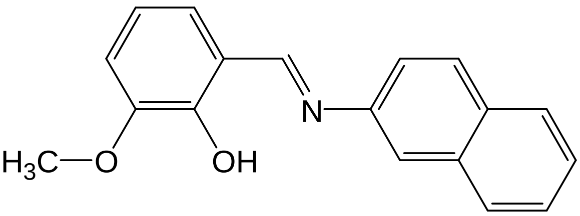	
Molecular formula	$C_{18}H_{15}NO_2$	
M_r	227.32	
Crystal system	Orthorhombic	
Space group	$P\ 2_12_12_1$	
T / K	298	110
Crystal data:		
a / Å	7.0652(4)	6.8518(4)
b / Å	11.3687(6)	11.3764(6)
c / Å	17.5723(8)	17.4137(8)
V / Å^3	1411.44(13)	1357.38(12)
Z	4	
D_{calc} / g cm^{-3}	1.305	1.357
λ(MoK_α) / Å	0.71073	
μ / mm^{-1}	0.085	0.089
Crystal size / mm^3	0.92 x 0.54 x 0.44	
F(000)	584	
Refl. collected/unique	5719 / 3055	5409 / 2933
Data/Restraints/Parameters	199	
$\Delta\rho_{\text{max}}$, $\Delta\rho_{\text{min}}$ / e Å^{-3}	0.093; –0.084	0.166; –0.132
$R[F^2 \geq 2\sigma(F^2)]$	0.0308	0.0294
$wR(F^2)$	0.0685	0.0759
Goodness-of-fit, S	0.851	1.080

Table S4. General and crystallographic data for **3a** at 298 and 110 K.

Structural formula	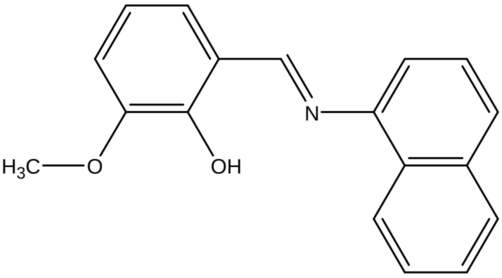	
Molecular formula	$C_{18}H_{15}NO_2$	
M_r	227.32	
Crystal system	Triclinic	
Space group	$P\bar{1}$	
T / K	298	110
Crystal data:		
a / Å	12.3034(4)	12.2742(3)
b / Å	15.4060(5)	15.2924(4)
c / Å	16.9536(4)	16.6009(5)
α / °	69.620(2)	69.246(3)
β / °	80.598(2)	80.702(2)
γ / °	70.170(3)	70.336(2)
V / Å^3	2829.99(15)	2740.73(13)
Z	8	
D_{calc} / g cm^{-3}	1.302	1.344
$\lambda(K_\alpha)$ / Å	1.54184 (Cu)	0.71073 (Mo)
μ / mm^{-1}	0.681	0.088
Crystal size / mm^3	0.70 x 0.60 x 0.30	
F(000)	1168	
Refl. collected/unique	28122 / 10182	22576 / 11715
Data/Restraints/Parameters	773	
$\Delta\rho_{max}$, $\Delta\rho_{min}$ / e Å^{-3}	0.159; –0.180	0.316; –0.209
$R[F^2 \geq 2\sigma(F^2)]$	0.0441	0.0386
$wR(F^2)$	0.1284	0.0857
Goodness-of-fit, S	1.039	0.824

Table S5. General and crystallographic data for **4** at 298 K.

Structural formula	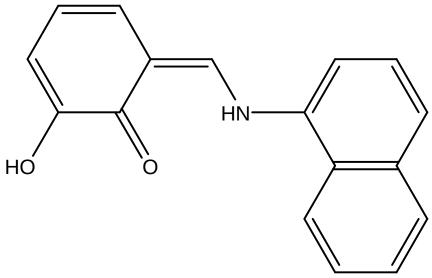
Molecular formula	$C_{17}H_{13}NO_2$
M_r	263.29
Crystal system	Monoclinic
Space group	$P\ 2_1/c$
Crystal data:	
a / Å	7.3959(6)
b / Å	23.9850(16)
c / Å	7.5966(6)
β / °	108.804(8)
V / Å^3	1275.64(17)
Z	4
D_{calc} / g cm^{-3}	1.371
$\lambda(\mathrm{Mo}K_\alpha)$ / Å	0.71073
μ / mm^{-1}	0.090
Crystal size / mm^3	0.95 x 0.90 x 0.40
$F(000)$	552
Refl. collected/unique	5942 / 2761
Data/Restraints/Parameters	191
$\Delta\rho_{max}$, $\Delta\rho_{min}$ / e Å^{-3}	0.151; –0.134
$R[F^2 \geq 2\sigma(F^2)]$	0.0400
$wR(F^2)$	0.0867
Goodness-of-fit, S	0.727

Table S6. General and crystallographic data for **5** at 298 and 110 K.

Structural formula	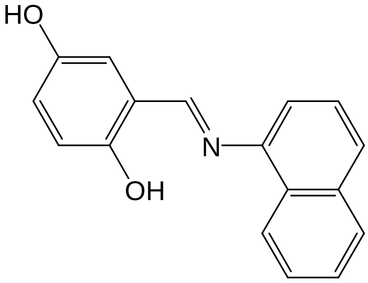	
Molecular formula	$C_{17}H_{13}NO_2$	
M_r	236.29	
Crystal system	Monoclinic	
Space group	$P\,2_1/c$	
T / K	298	110
Crystal data:		
a / Å	11.9699(6)	11.9796(4)
b / Å	10.1432(7)	9.9836(4)
c / Å	11.0736(7)	10.9926(4)
β / °	103.312(5)	103.664(4)
V / Å^3	1308.35(14)	1277.50(8)
Z	4	
D_{calc} / g cm^{-3}	1.337	1.369
$\lambda(K_\alpha)$ / Å	0.71073	
μ / mm^{-1}	0.088	0.090
Crystal size / mm^3	0.95 x 0.90 x 0.40	
$F(000)$	552	
Refl. collected/unique	5765 / 2802	5576 / 2750
Data/Restraints/Parameters	188	
$\Delta\rho_{max}$, $\Delta\rho_{min}$ / e Å^{-3}	0.170; –0.193	0.290; –0.253
$R[F^2 \geq 2\sigma(F^2)]$	0.0380	0.0347
$wR(F^2)$	0.1153	0.0958
Goodness-of-fit, S	1.091	1.071

Table S7. General and crystallographic data for **6** at 110 K.

Structural formula	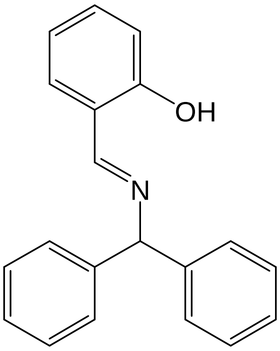
Molecular formula	$C_{20}H_{17}NO$
M_r	287.36
Crystal system	Monoclinic
Space group	$P\ 2_1$
Crystal data:	
a / Å	8.5081(3)
b / Å	6.0774(2)
c / Å	15.4176(6)
β / °	99.982(3)
V / Å^3	758.74(4)
Z	2
D_{calc} / g cm^{-3}	1.258
λ(MoK_α) / Å	0.71073
μ / mm^{-1}	0.077
Crystal size / mm^3	0.40 x 0.32 x 0.20
F(000)	304
Refl. collected/unique	6551 / 3106
Data/Restraints/Parameters	202
$\Delta\rho_{max}$, $\Delta\rho_{min}$ / e Å^{-3}	0.174, –0.170
$R[F^2 \geq 2\sigma(F^2)]$	0.0302
$wR(F^2)$	0.0688
Goodness-of-fit, S	1.003

Table S8. General and crystallographic data for **7** at 298 and 110 K.

Structural formula	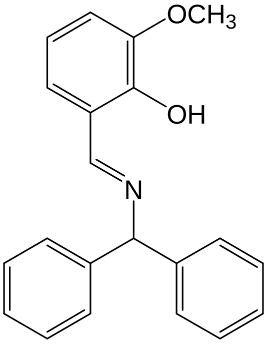	
Molecular formula	$C_{21}H_{19}NO_2$	
M_r	317.38	
Crystal system	Monoclinic	
Space group	$P\ 2_1/c$	
T / K	298	110
Crystal data:		
a / Å	11.756(2)	11.6407(8)
b / Å	12.176(2)	12.0666(9)
c / Å	12.2037(19)	12.0964(8)
β / °	91.224(15)	91.535(7)
V / Å^3	1746.5(5)	1698.5(2)
Z	4	
D_{calc} / g cm^{-3}	1,207	1,241
$\lambda(K_\alpha)$ / Å	0.71073	
μ / mm^{-1}	0,077	0,080
Crystal size / mm^3	0.75 x 0.25 x 0.15	
$F(000)$	672	
Refl. collected/unique	7909 / 3739	7718 / 3332
Data/Restraints/Parameters	222	
$\Delta\rho_{max}$, $\Delta\rho_{min}$ / e Å^{-3}	0.091; –0.101	0.229; –0.288
$R[F^2 \geq 2\sigma(F^2)]$	0.0342	0.0531
$wR(F^2)$	0.0613	0.1312
Goodness-of-fit, S	0.603	1.045

Table S9. Values of O1–C2 and N1–C7 bond lengths for **1**-**7** used for tautomer determination. (RT = 298 K, LT = 110 K)

Compound		**Interatomic distance, *d* / Å**	
		RT	**LT**
1	O1–C2	1.354(2)	1.3573(16)
	N1–C7	1.283(2)	1.2839(18)
2	O1–C2	1.3551(17)	1.3466(14)
	N1–C7	1.2809(18)	1.2846(16)
3a	O11–C12	1.3479(15)	1.3506(17)
	N11–C17	1.2789(16)	1.2837(18)
	O21–C22	1.3470(15)	1.3505(17)
	N21–C27	1.2770(16)	1.2795(18)
	O31–C32	1.3483(14)	1.3481(16)
	N31–C37	1.2787(17)	1.2828(18)
	O41–C42	1.3535(19)	1.3584(18)
	N41–C47	1.2743(17)	1.2727(18)
4	O1–C2	1.302(2)	1.296(2)
	N1–C7	1.305(2)	1.313(3)
5	O1–C2	1.3679(14)	1.3697(13)
	N1–C7	1.2748(15)	1.2806(14)
6	O1–C2	1.3594(16)	1.3577(14)
	N1–C7	1.2718(16)	1.2775(15)
7	O1–C2	1.353(2)	1.347(2)
	N1–C7	1.267(2)	1.279(2)

Table S10. Intermolecular Hydrogen-bond geometry (Å, °).
D – donor atom, *A* – acceptor atom. (RT = 298 K, LT = 110 K)

Compound		**H-bond type**	***d*(*D*···*A*) / Å**	**∡(*D*–H···*A*) / °**	**Symmetry operator**
1	RT	C5–H5···O1^{i}	3.480(3)	119.97(15)	(i) *x* – ½, –*y* + 1, *z*
	LT		3.403(2)	119.41(9)	
2	RT	C4–H4···O2^{i}	3.505(2)	157.08(10)	(i) *x* + ½, –*y* + ½ + 1, –*z*
	LT		3.417(2)	153.62(8)	
	RT	C9–H9···O2^{ii}	3.405(2)	122.41(10)	(ii) –*x* + 2, +*y* + ½, –*z* + ½
	LT		3.280(2)	117.49(8)	
	RT	C12–H12···O2^{iii}	3.490(2)	139.79(11)	(iii) –*x* + 1, +*y* + ½, –*z* + ½
	LT		3.418(2)	139.10(8)	
	RT	C10–H10···O1^{iii}	3.380(2)	119.93(10)	
	LT		3.328(2)	119.22(8)	
	LT	C12–H12···O1^{iii}	3.462(2)	116.78(8)	
3a	RT	C218–H28C···O32	3.334(3)	119.14(11)	(i) –*x* + 1, –*y*, –*z* + 1
	LT		3.274(2)	118.03(10)	
	RT	C19–H19···O22	3.515(2)	166.13(9)	
	LT		3.446(2)	165.42(10)	
	RT	CLT–HLT···O21	3.455(2)	136.30(10)	
	LT		3.417(2)	135.44(10)	
	RT	C210–H210···O11	3.451(2)	138.40(11)	(ii) –*x*, –*y* + 1, –*z* + 1
	LT		3.400(2)	136.99(11)	
	RT	C39–H39···O41	3.426(2)	128.88(11)	(iii) –*x* + 1, –*y*, –*z*
	LT		3.389(2)	126.68(11)	
4	RT	O2–H2···O1^{i}	2.737(2)	108(2)	(i) *x*, *y*, *z*
	LT		2.749(2)	109(2)	
	RT	C7–H7···O2^{ii}	3.385(2)	130.26(12)	(ii) *x* – 1, +*y*, +*z*
	LT		3.268(3)	131.54(15)	
	LT	C9–H9···O1^{ii}	3.464(3)	112.73(15)	
5	RT	O2–H2···O1^{i}	2.538(1)	171(2)	(i) *x* – ½, –*y* + ½, –*z*
	LT		2.533(1)	169(2)	
	RT	C3–H3···O2^{ii}	3.554(2)	120.46(8)	(ii) *x* + ½, –*y* + ½, –*z*
	LT		3.538(1)	120.05(7)	
	RT	C9–H9···O2^{iii}	3.411(2)	172.53(9)	(iii) –*x* + ½ + 1, –*y* + 1, +*z* + ½
	LT		3.384(1)	173.88(7)	
	RT	C9–H9···O1^{iv}	3.595(2)	131.74(10)	(iv) –*x* + ½ + 2, –*y* + 1, +*z* + ½
	LT		3.507(1)	130.11(7)	

Continued on the next page…

Table S10. – continued from the previous page. Intermolecular Hydrogen-bond geometry (Å, °).
D – donor atom, *A* – acceptor atom.

Compound	*T* / K	H-bond type	*d(D···A) / Å*	∡(*D*–H···*A*) / °	Symmetry operator
6	RT	C7–H7···O1^{i}	3.545(2)	132.81(9)	(i) *x*, +*y*–1, +*z*
	LT		3.467(2)	131.41(8)	
	RT	C20–H20···O1^{i}	3.550(2)	2.721(1)	
	LT		3.522(2)	147.33(8)	
7	RT	C7–H7···O2^{i}	3.360(3)	133.40(13)	(i) *x*, –*y* + ½ + 1, +*z* + ½
	LT		3.335(2)	133.32(10)	
	RT	C8–H8···O1^{i}	3.297(2)	160.07(12)	
	LT		3.232(2)	158.19(10)	
	RT	C20–H20···O2^{i}	3.524(3)	145.84(15)	
	LT		3.443(3)	146.58(14)	

Table S11. Dihedral angle values for **1–7** at RT and LT. (*) The value for the dihedral angles involving the aldehyde ring and each phenyl ring separately. (**)Values taken from the CSD or from the references.

Compound	*dihedral angle* / °	
	RT	**LT**
1	8.24(5)	8.70(4)
1**	8.09(10)	-
2	14.23(4)	14.14(4)
3a	33.21(4) 31.49(4) 27.95(4) 22.44(5)	31.74(4) 29.99(4) 27.78(4) 21.21(5)
3b**	10.10(4) 11.54(4)	-
4	5.03(5)	5.64(6)
4**	-	5.87(8)
5	56.34(3)	54.68(3)
6*	62.11(5) 72.93(5)	61.20(4) 74.59(4)
6**	62.072 72.969	-
7*	63.81(8) 63.22(9)	64.16(6) 63.53(7)

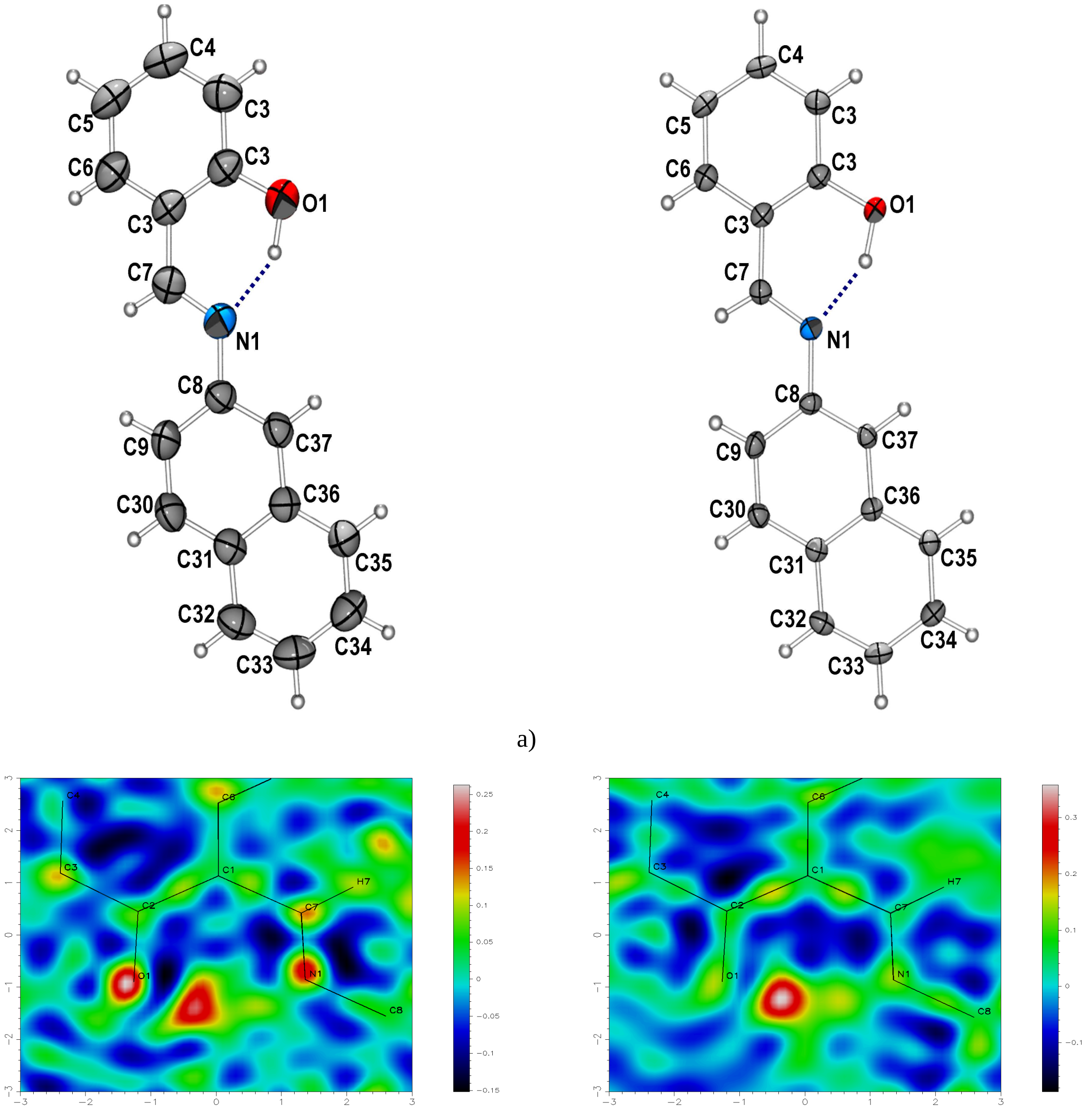

a)

b)

Figure S8. a) Thermal ellipsoid (50 %) plot of the enol-imine tautomeric form of **1** showing the atom-labelling scheme. Dashed line indicates intramolecular interaction. Data obtained at 298 (left) and 110 K (right). b) δF maps calculated through N1–C7–C1–C2–O1 chelate ring of **1** at 298 (left) and 110 K (right).

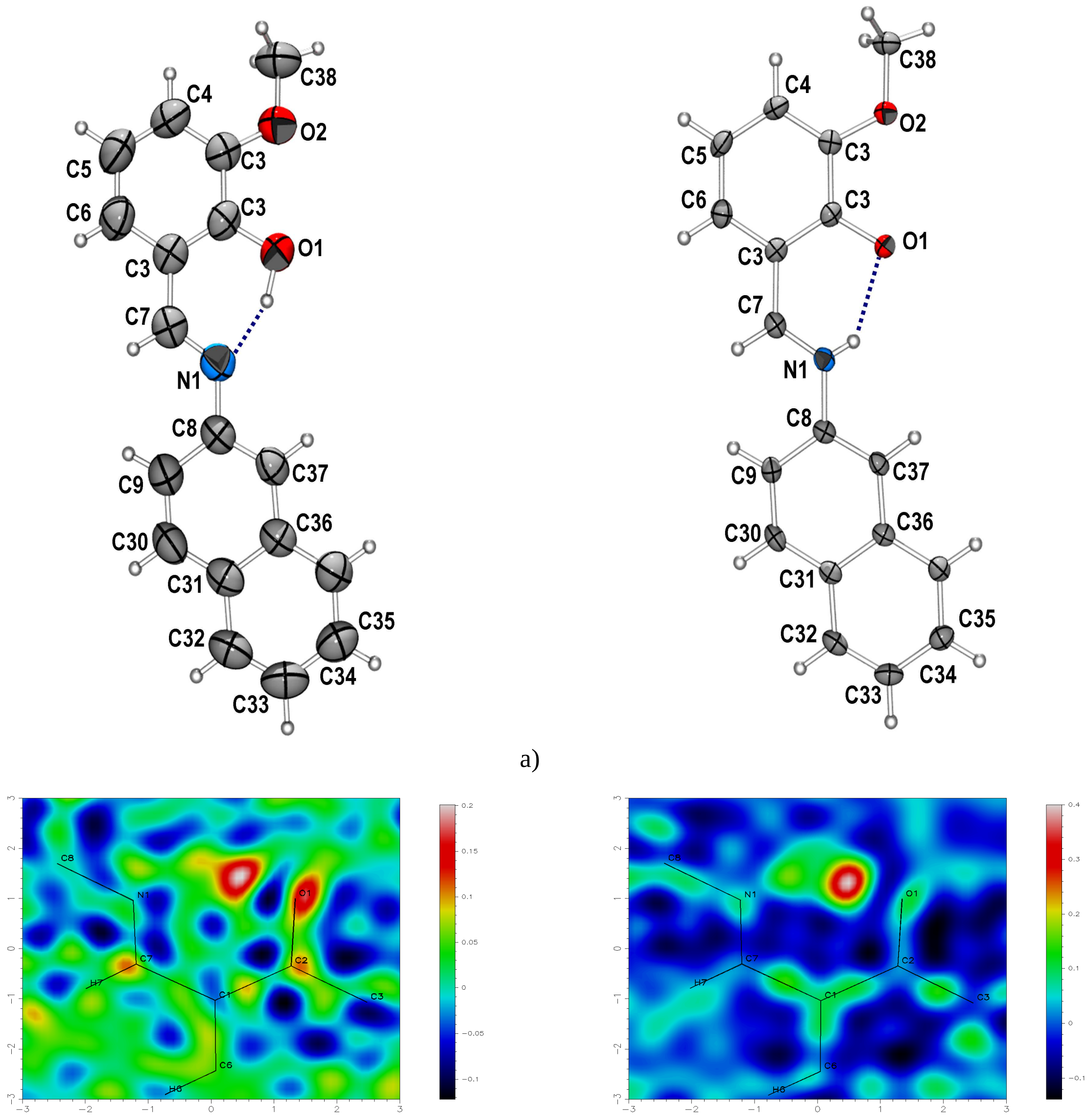

a)

b)

Figure S9. a) Thermal ellipsoids (50 %) plot of the enol-imine tautomeric forms of **2** showing the atom-labelling scheme. Dashed lines indicate intramolecular interactions. Data obtained at 298 (left) and 110 K (right). b) δF maps calculated through N1–C7–C1–C2–O1 chelate ring of **2** at 298 (left) and 110 K (right).

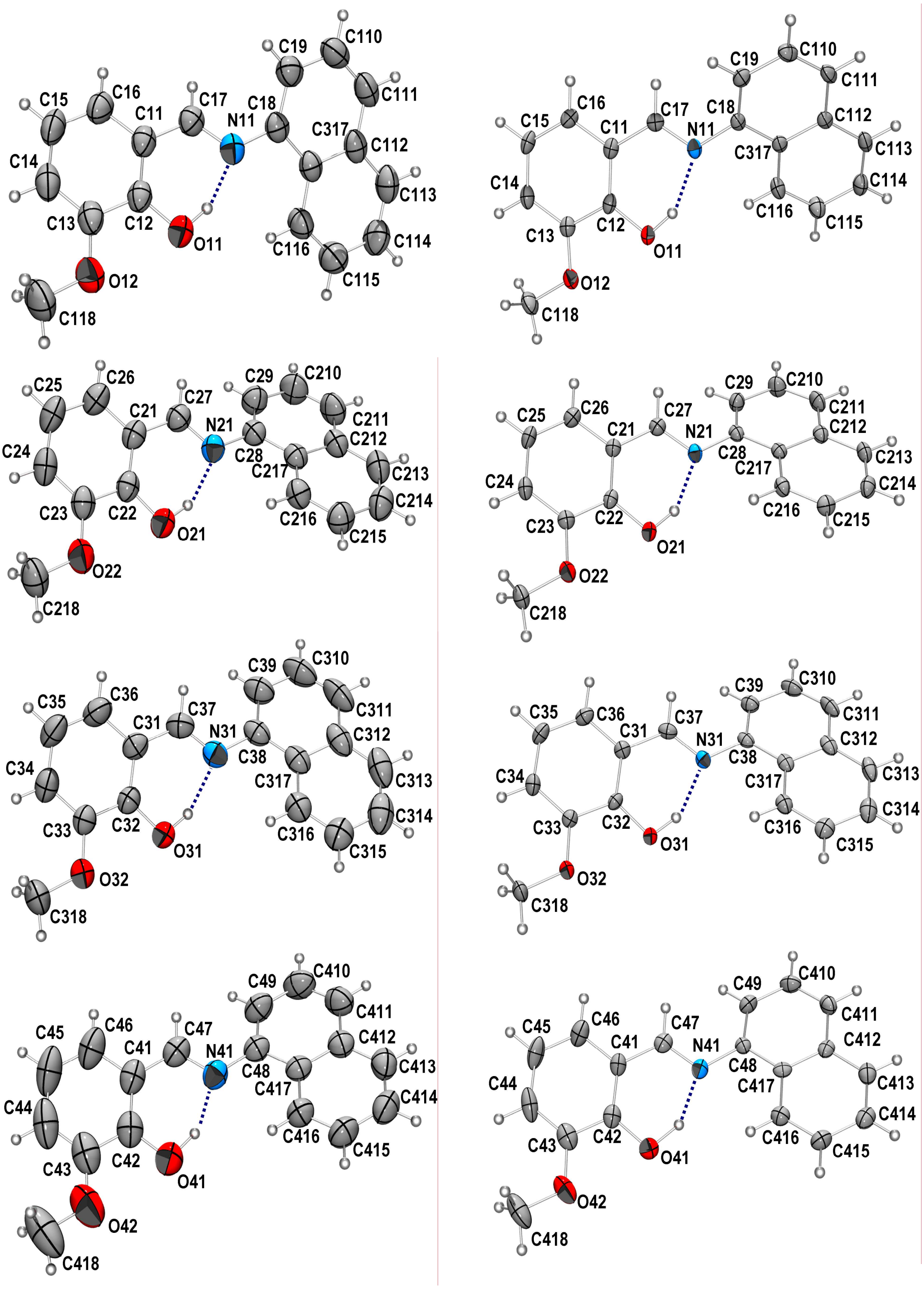

a)

Figure S10. a) Thermal ellipsoids (50 %) plot of the enol-imine tautomeric forms of **3a** showing the atom-labelling scheme. Dashed lines indicate intramolecular interactions. Data obtained at 298 (left) and 110 K (right).

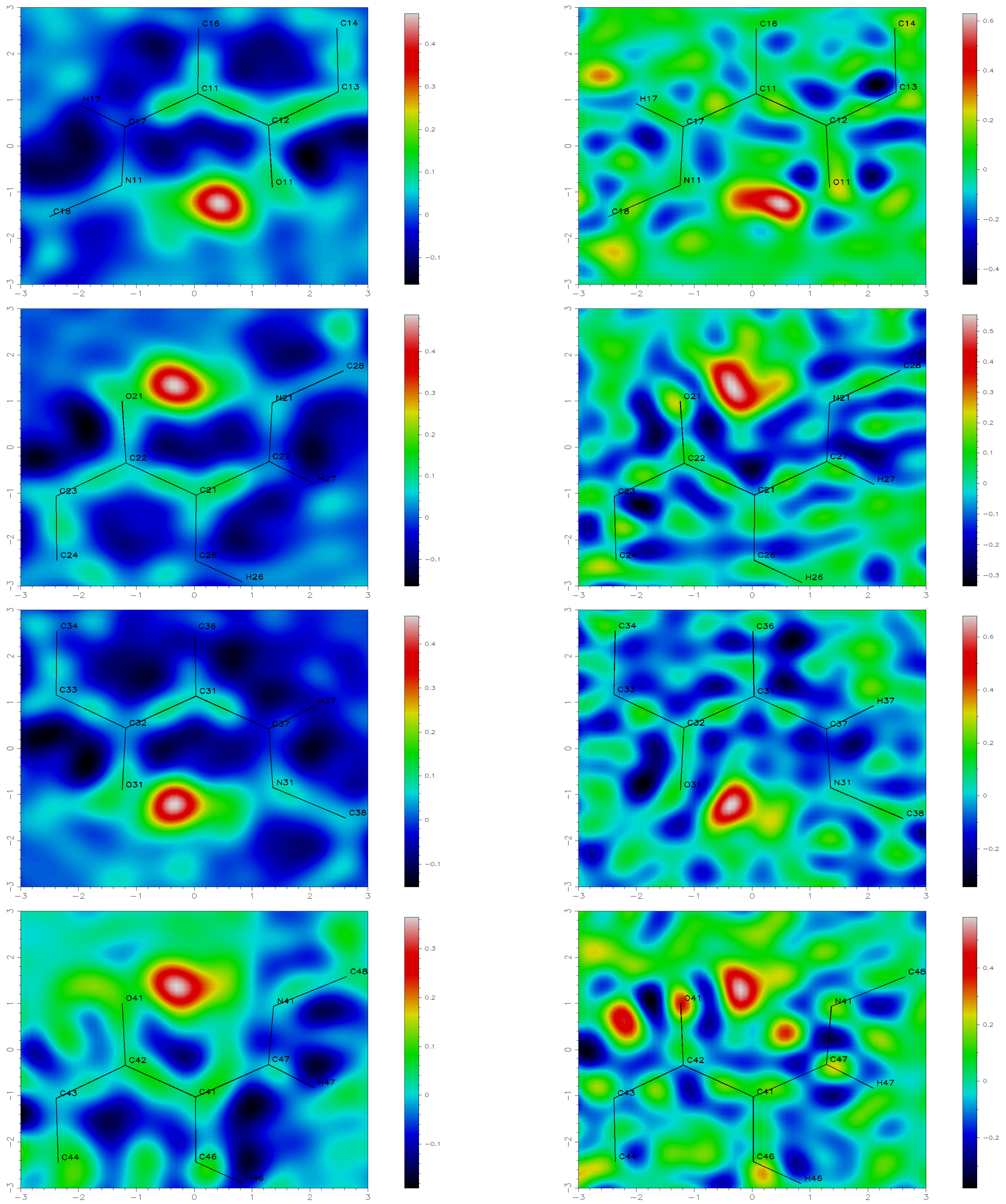

b)

Figure S10. b) δF maps calculated through N1–C7–C1–C2–O1 chelate ring of **3a** at 298 (left) and 110 K (right).

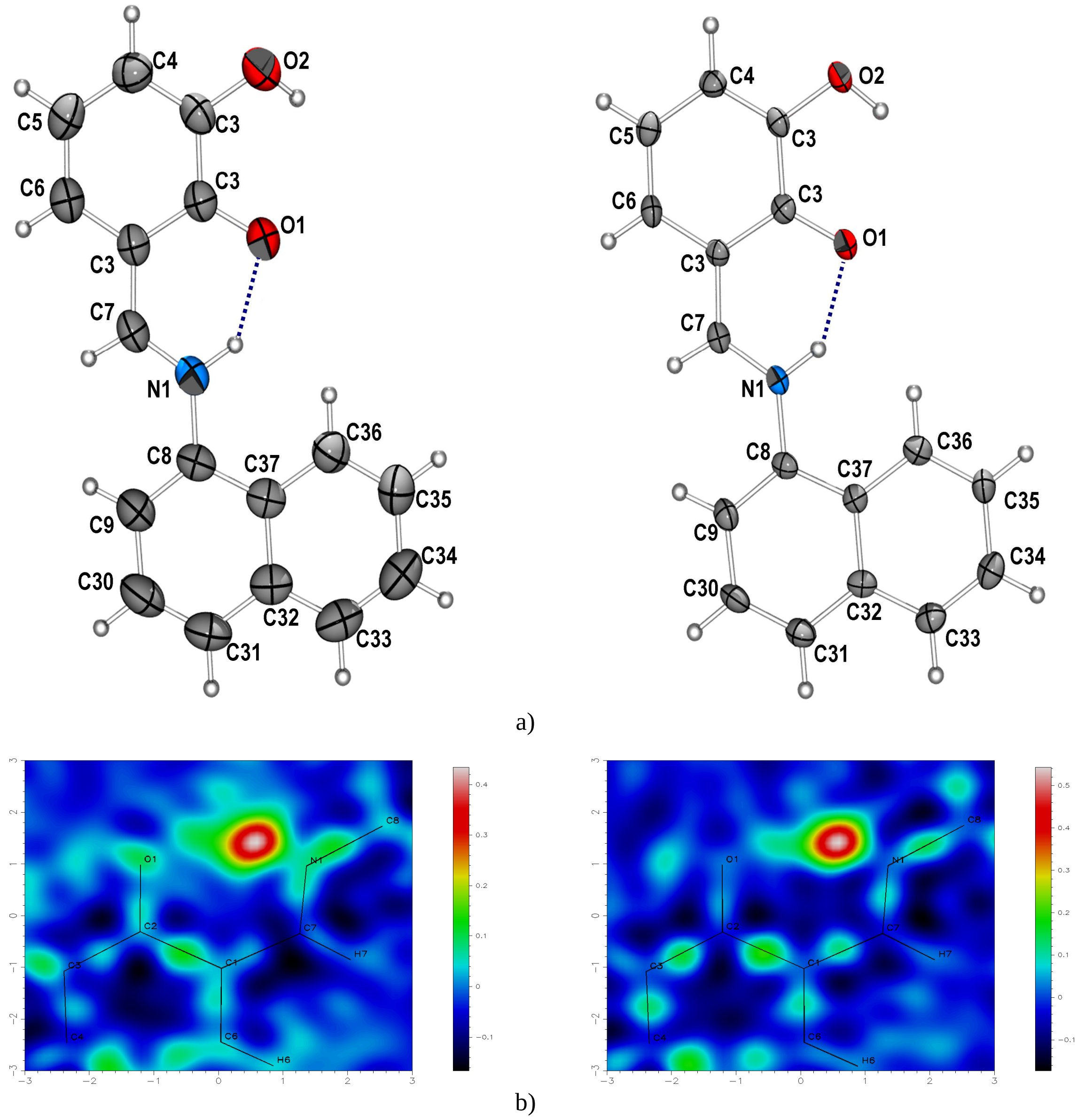

Figure S11. a) Thermal ellipsoids (50 %) plot of the keto-amine tautomeric forms of **4** showing the atom-labelling scheme. Dashed lines indicate intramolecular interactions. Data obtained at 298 (left) and 110 K (right). b) δF maps calculated through N1–C7–C1–C2–O1 chelate ring of **4** at 298 (left) and 110 K (right).

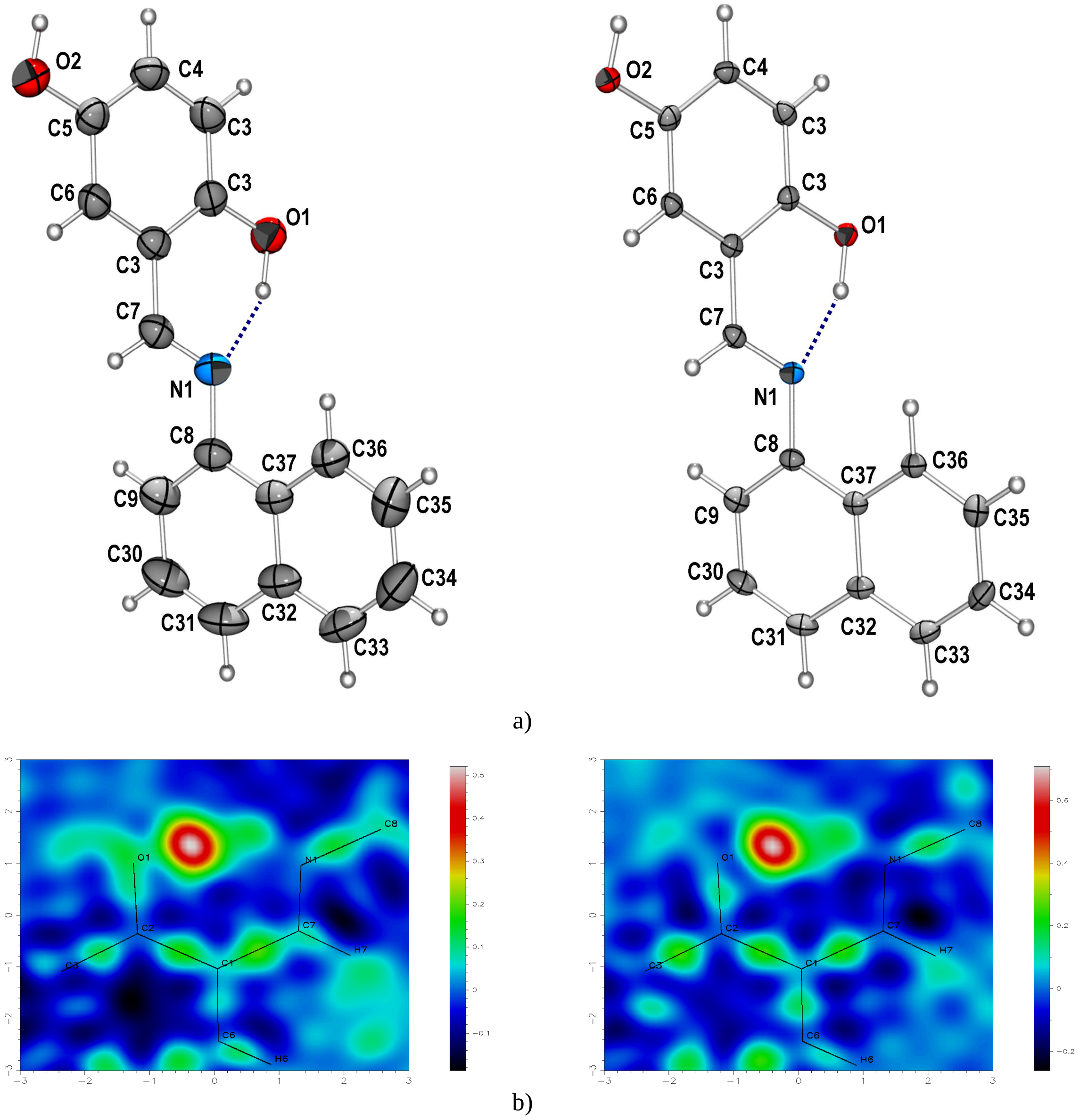

Figure S12. a) Thermal ellipsoids (50 %) plot of the enol-imine tautomeric forms of **5** showing the atom-labelling scheme. Dashed lines indicate intramolecular interactions. Data obtained at 298 (left) and 110 K (right). b) *δ*F maps calculated through N1–C7–C1–C2–O1 chelate ring of **5** at 298 (left) and 110 K (right).

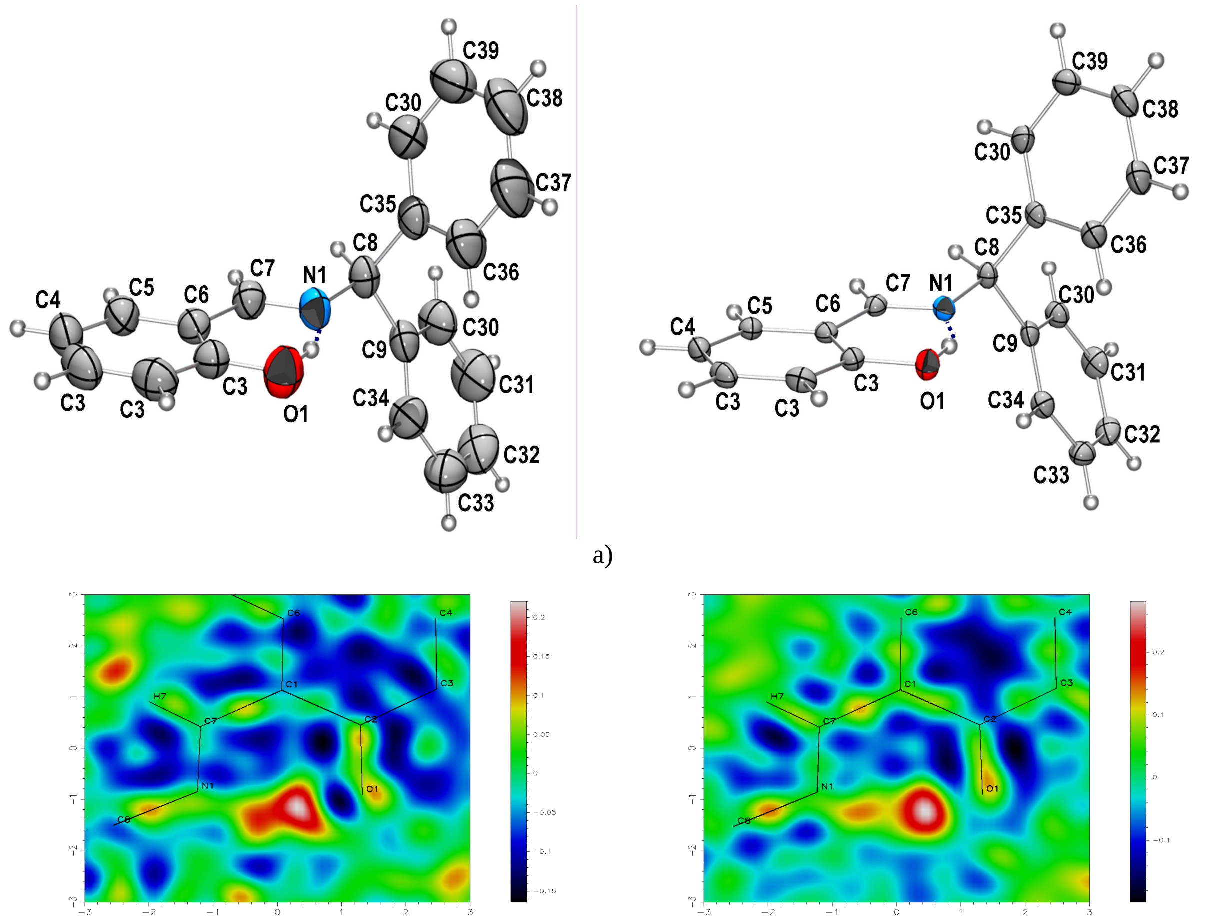

Figure S13. a) Thermal ellipsoids (50 %) plot of the enol-imine tautomeric forms of **6** showing the atom-labelling scheme. Dashed lines indicate intramolecular interactions. Data obtained at 298 (left) and 110 K (right). b) δF maps calculated through N1–C7–C1–C2–O1 chelate ring of **6** at 298 (left) and 110 K (right).

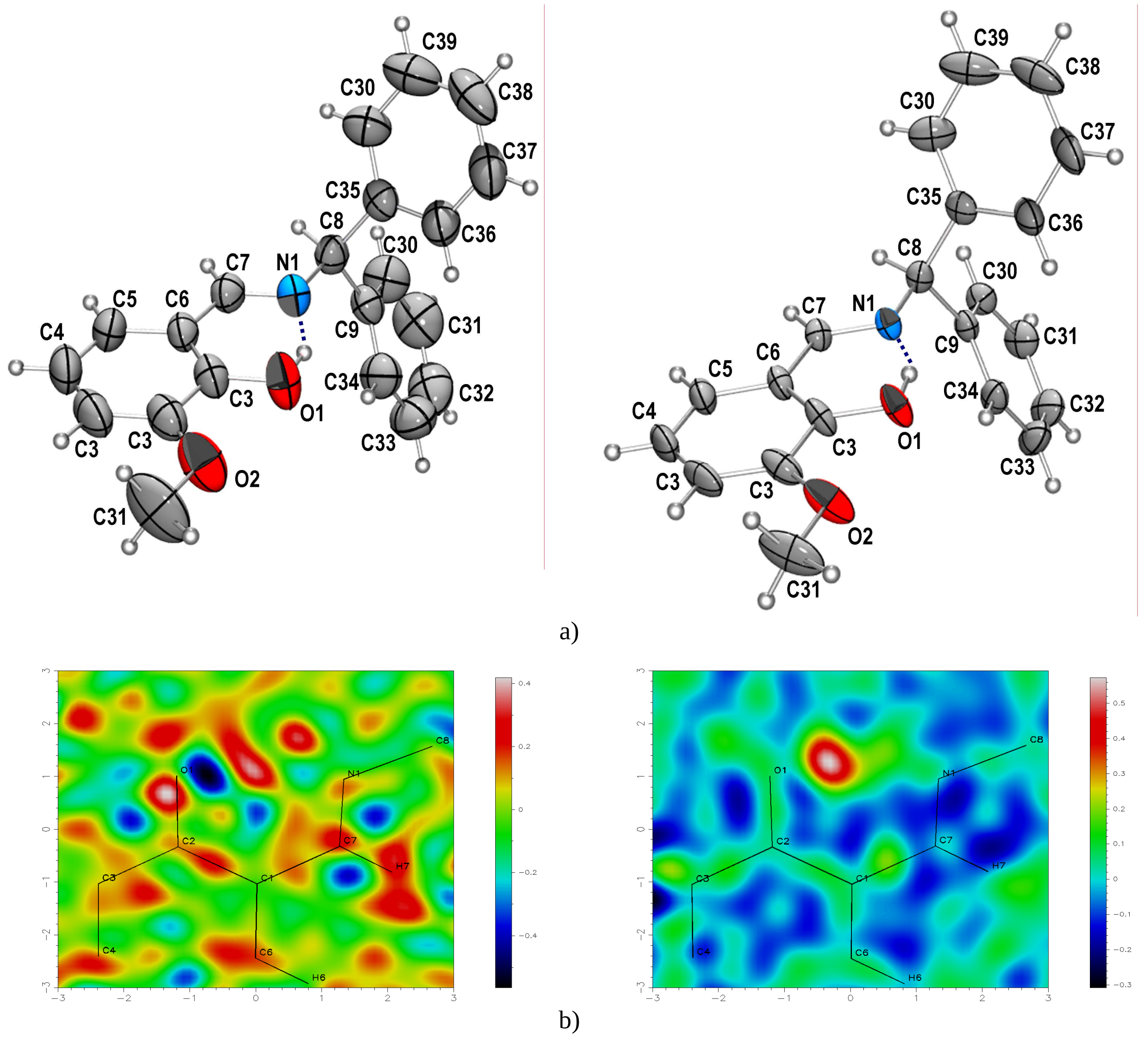

Figure S14. a) Thermal ellipsoids (50 %) plot of the enol-imine tautomeric forms of **7** showing the atom-labelling scheme. Dashed lines indicate intramolecular interactions. Data obtained at 298 (left) and 110 K (right). b) *δ*F maps calculated through N1–C7–C1–C2–O1 chelate ring of **7** at 298 (left) and 110 K (right).

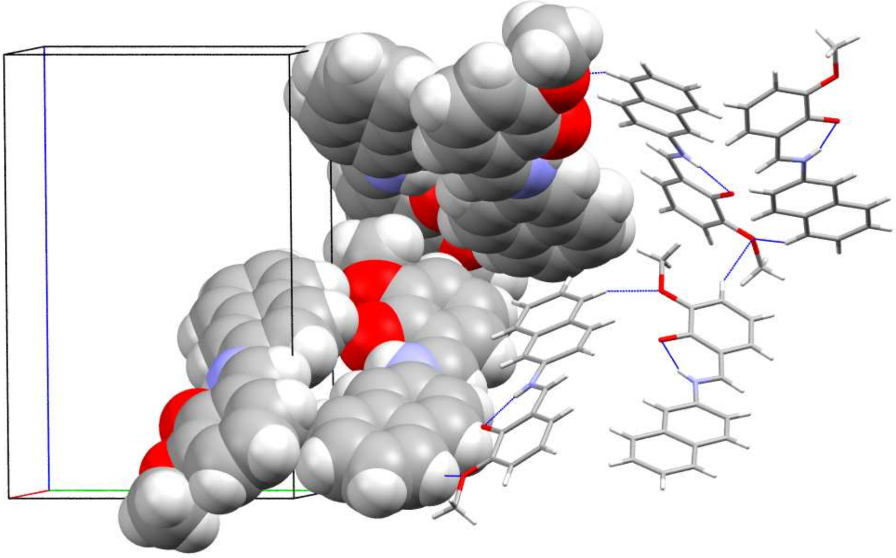

Figure S15. View of the 2D supramolecular network formed by means of interactions between the molecules of **2**. Blue dotted lines indicate the interactions.

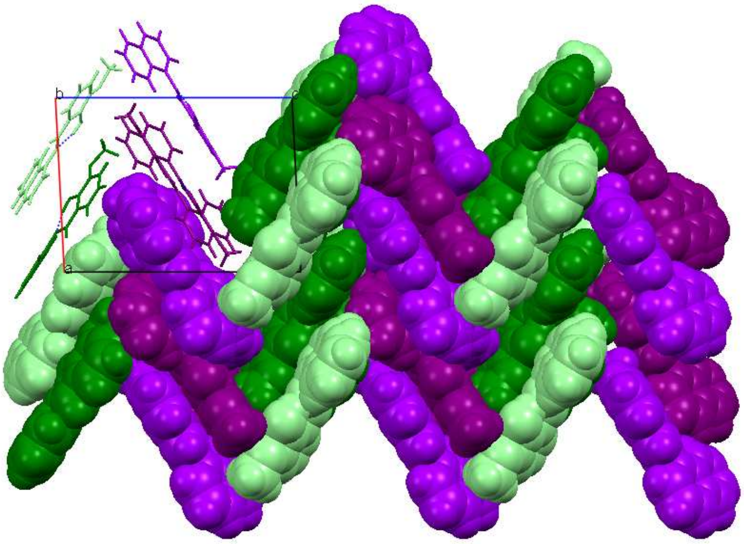

Figure S16. View of the 3D supramolecular network formed by means of interactions between the molecules of **3a**.

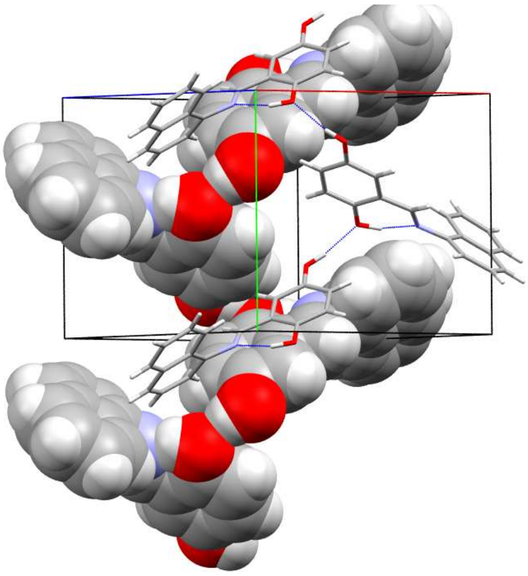

Figure S17. View of the 1D-helices formed by means of interactions between the molecules of **5**. Blue dotted lines indicate the interactions.

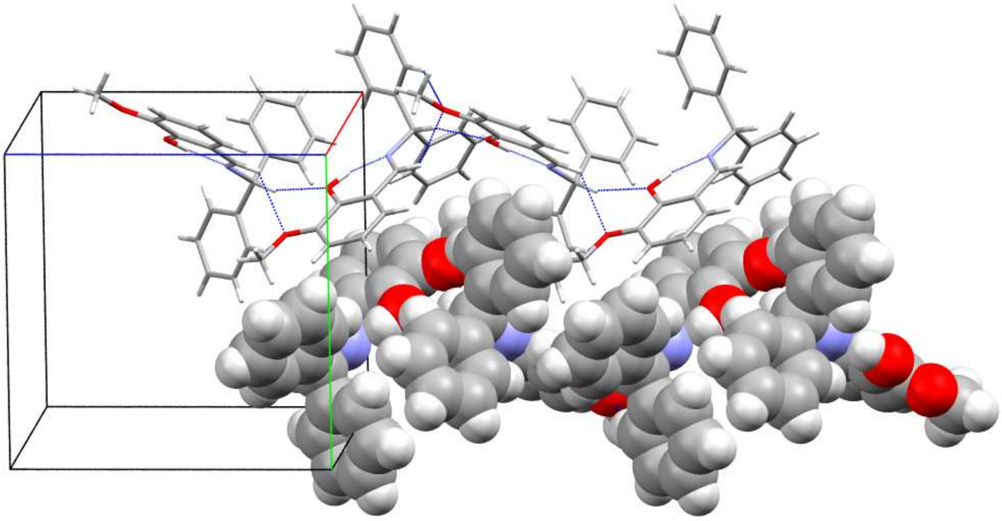

Figure S18. View of the 1D-helices formed by means of interactions between the molecules of **7**. Blue dotted lines indicate the interactions.

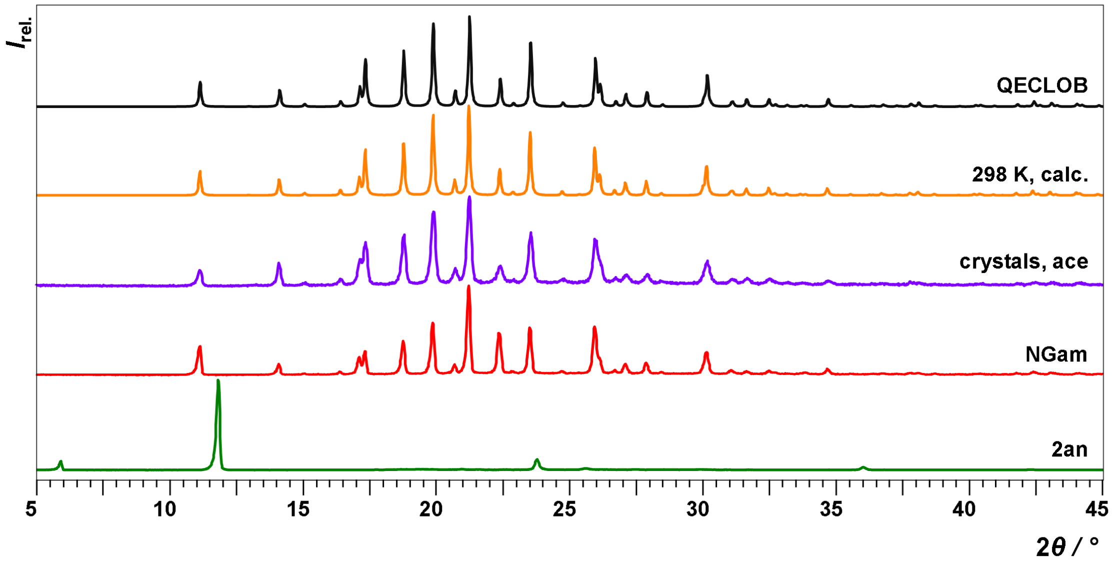

Figure S19. PXRD patterns of: pure **2an** reactant, product obtained by neat grinding in the mortar (**NGam**), bulk crystals obtained by slow evaporation of acetone, the calculated patterns of **1** and QECLOB [1], respectively.

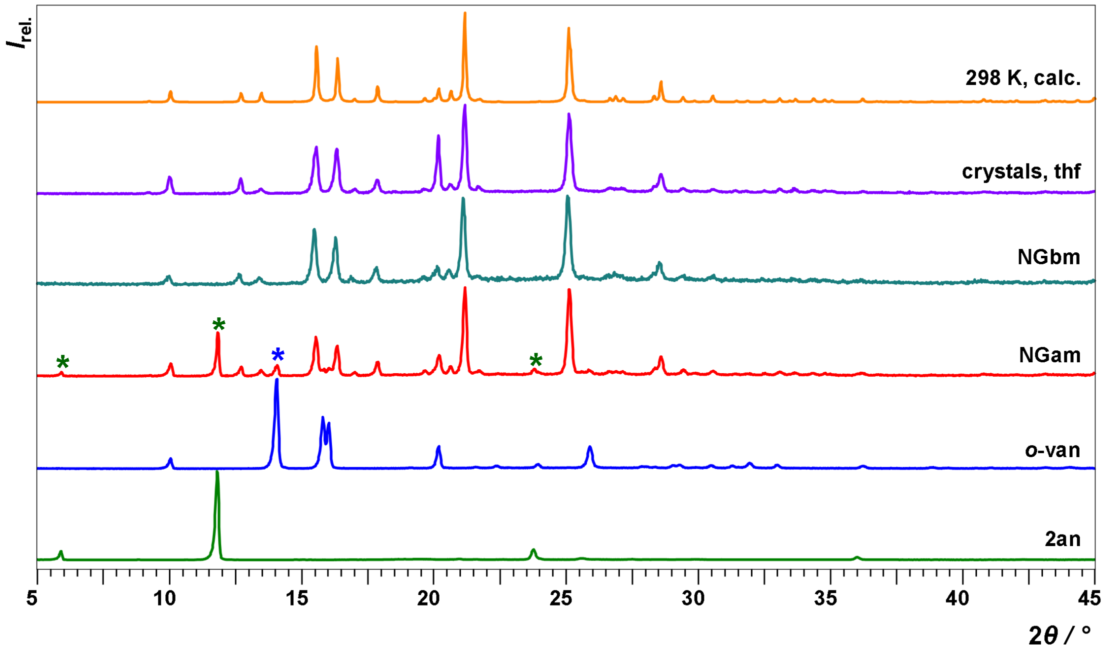

Figure S20. PXRD patterns of: pure **2an** reactant, pure ***o*-van** reactant, product obtained by neat grinding in the mortar (**NGam**), product obtained by neat grinding in the ball mill (**NGbm**), bulk crystals obtained by slow evaporation of tetrahydrofurane and the calculated pattern of **2**.

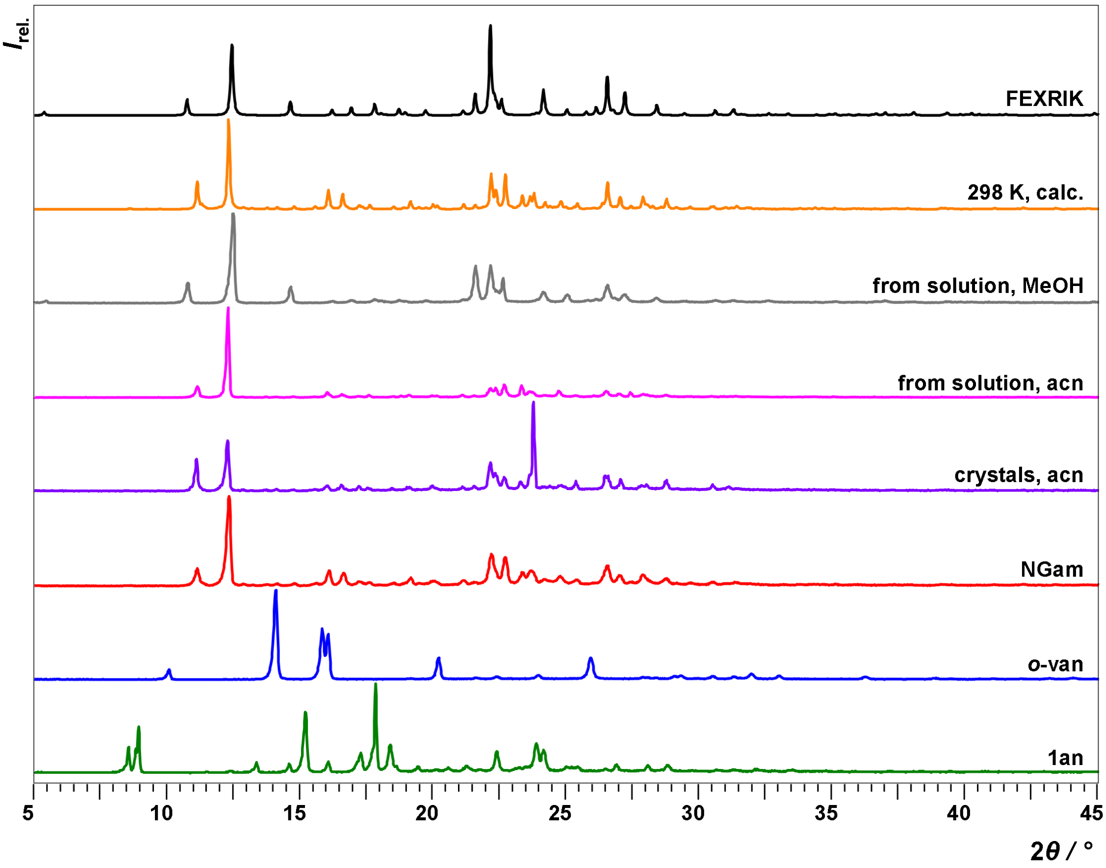

Figure S21. PXRD patterns of: pure **1an** reactant, pure ***o*-van** reactant, product obtained by neat grinding in the mortar (**NGam**), bulk crystals obtained by slow evaporation of acetonitrile, product obtained by solution synthesis in acetonitrile, product obtained by solution synthesis in methanol, the calculated patterns of **3a** and FEXRIK [2] (**3b**), respectively.

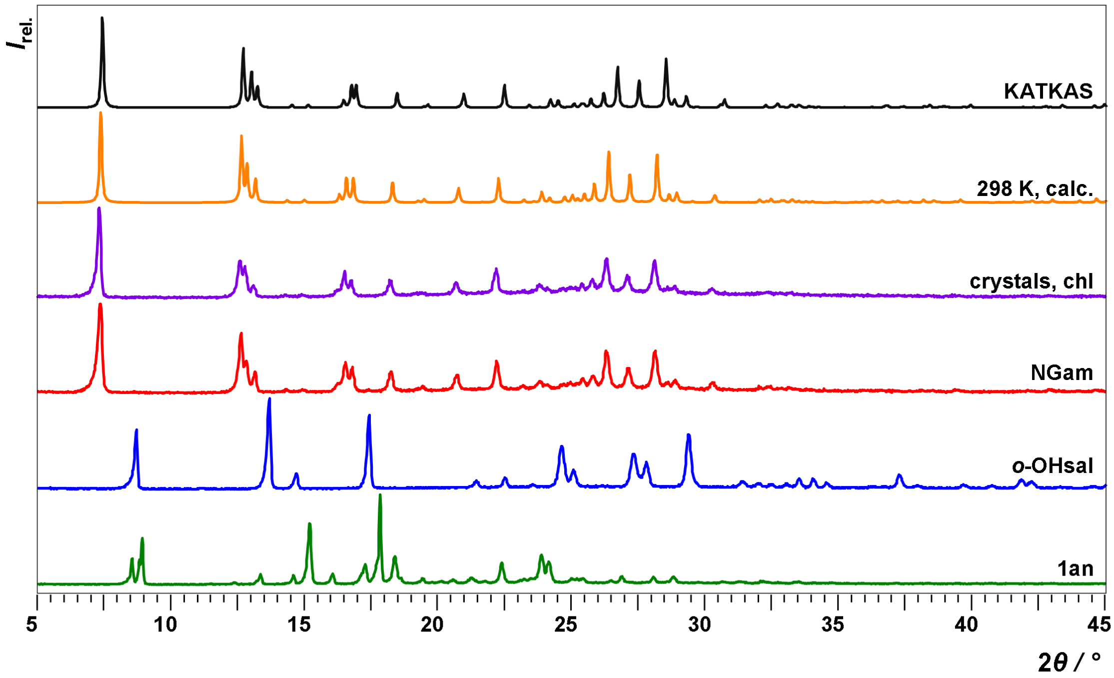

Figure S22. PXRD patterns of: pure **1an** reactant, pure ***o*-OHsal** reactant, product obtained by neat grinding in the mortar (**NGam**), bulk crystals obtained by slow evaporation of chloroform, the calculated patterns of **4** and KATKAS [3], respectively.

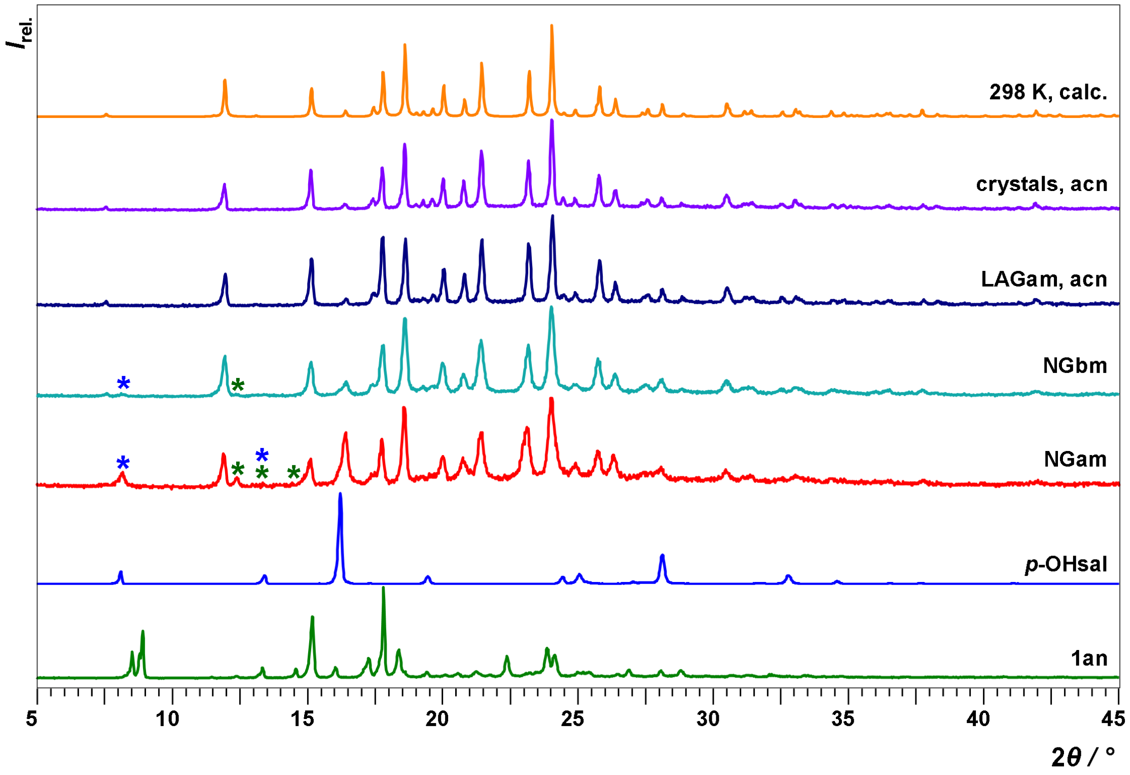

Figure S23. PXRD patterns of: pure **1an** reactant, pure ***p*-OHsal** reactant, product obtained by neat grinding in the mortar (**NGam**), product obtained by liquid (acetonitrile) assisted grinding in the mortar (**LAGam, acn**), bulk crystals obtained by slow evaporation of acetonitrile and the calculated pattern of **5.**

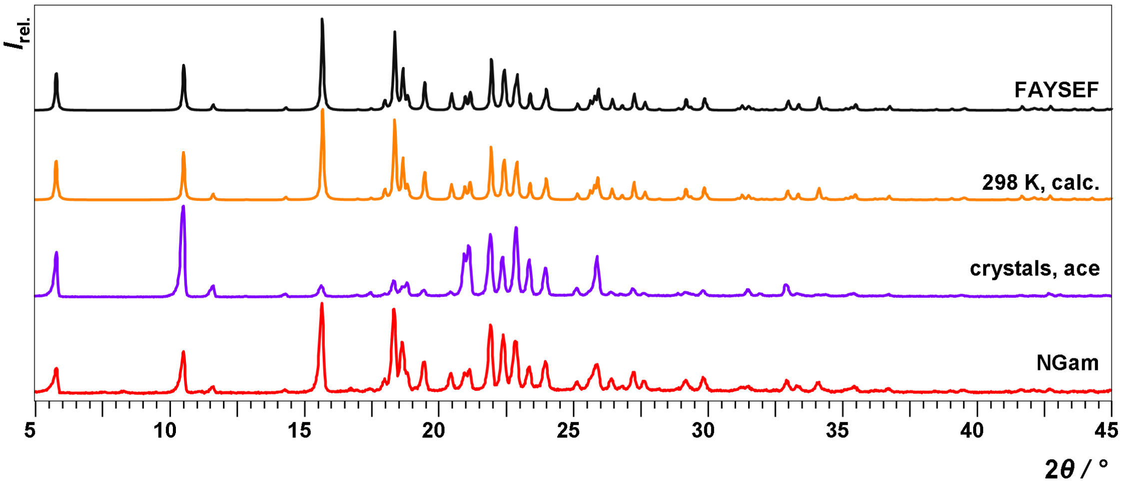

Figure S24. PXRD patterns of: product obtained by neat grinding in the mortar (**NGam**), bulk crystals obtained by slow evaporation of acetone and the calculated patterns of **6** and FAYSEF [4], respectively.

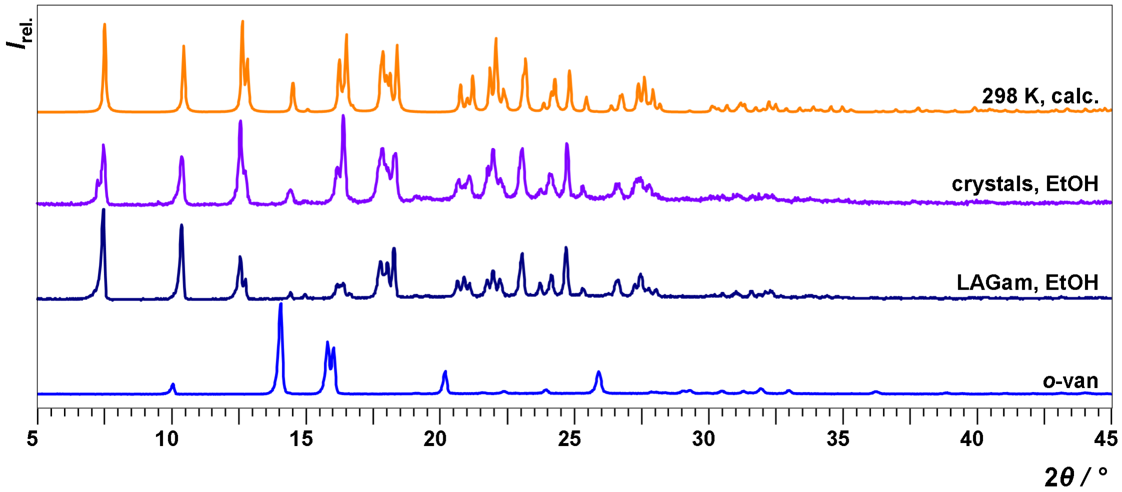

Figure S25. PXRD patterns of: pure ***o*-van** reactant, product obtained by neat grinding in the mortar (**NGam**), bulk crystals obtained by slow evaporation of ethanol and the calculated pattern of **7** and the calculated pattern of FASYEF [4].

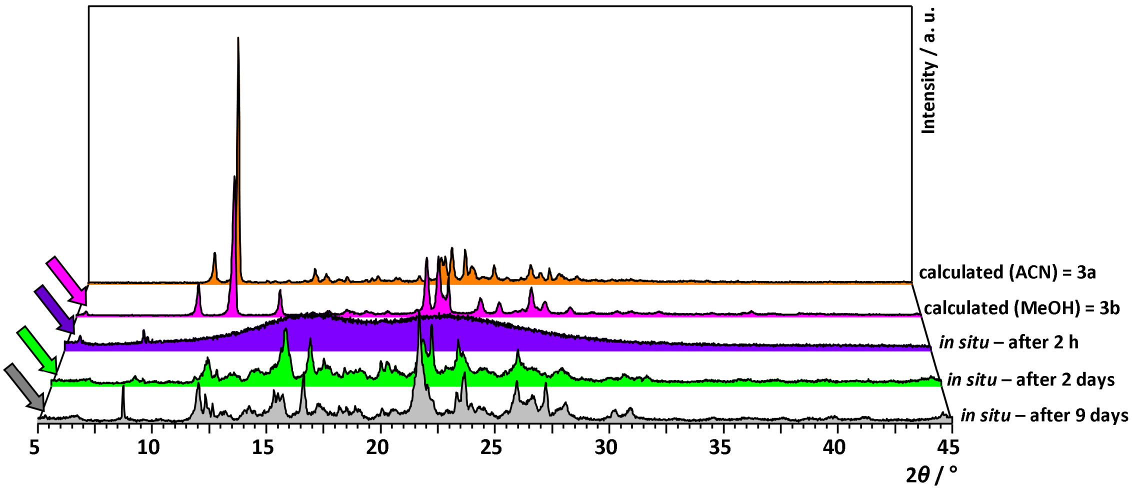

Figure S26. The calculated diffraction patterns of **3a** and **3b**, and the patterns obtained by *in-situ* PXRD monitoring of a close contact reaction of ***o*-van** and **1an**.

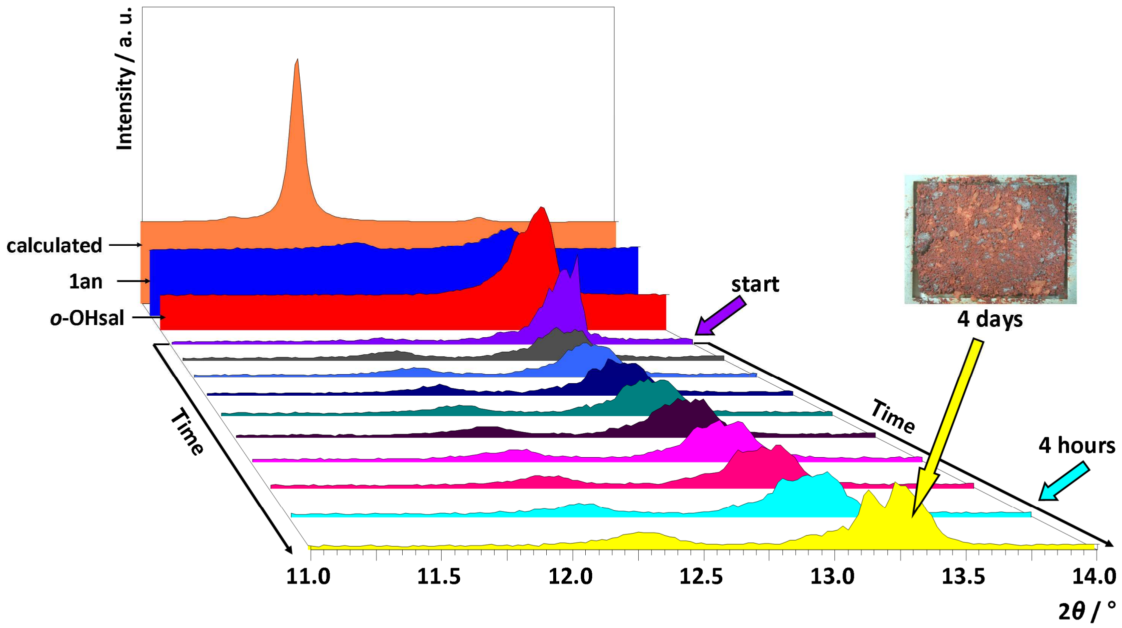

Figure S27. The calculated diffraction patterns of **5** and the patterns obtained by *in-situ* PXRD monitoring of a close contact reaction of ***p*-OHsal** and **1an**.

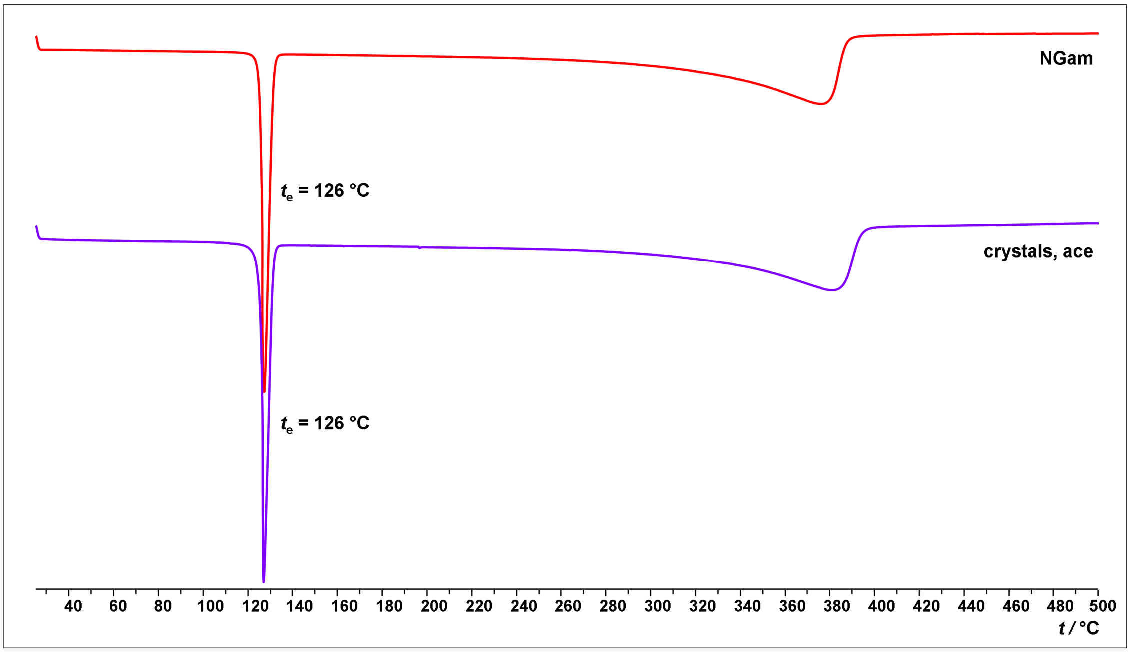

Figure S28. DSC curves for the bulk crystals of **1** obtained by slow evaporation of acetone and of the product obtained by neat grinding in the mortar (**NGam**).

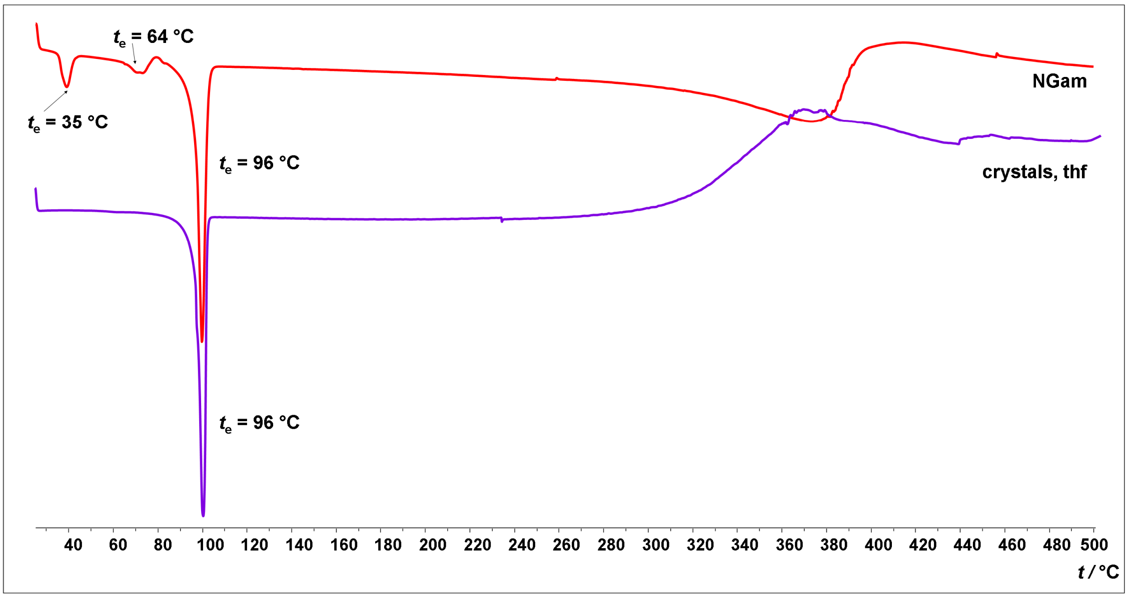

Figure S29. DSC curves for the bulk crystals of **2** obtained by slow evaporation of tetrahydrofurane and of the product obtained by neat grinding in the mortar (**NGam**).

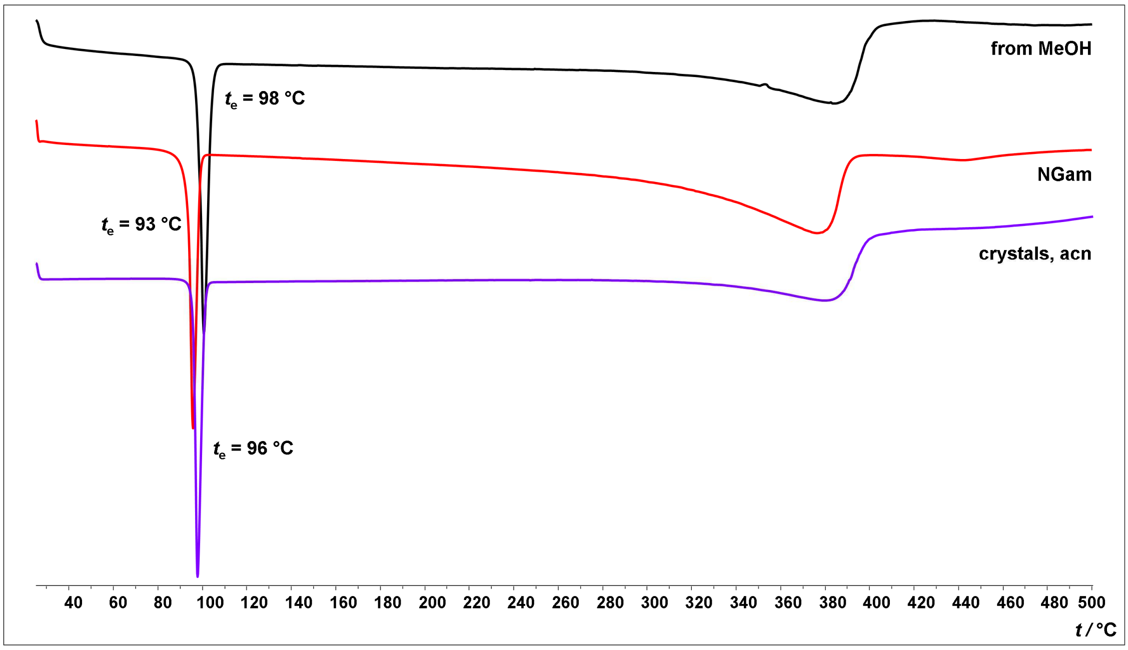

Figure S30. DSC curves for the bulk crystals of **3a** obtained by slow evaporation of acetonitrile, of the product obtained by neat grinding in the mortar (**NGam**) and the product obtained by solution synthesis in methanol (**3b**).

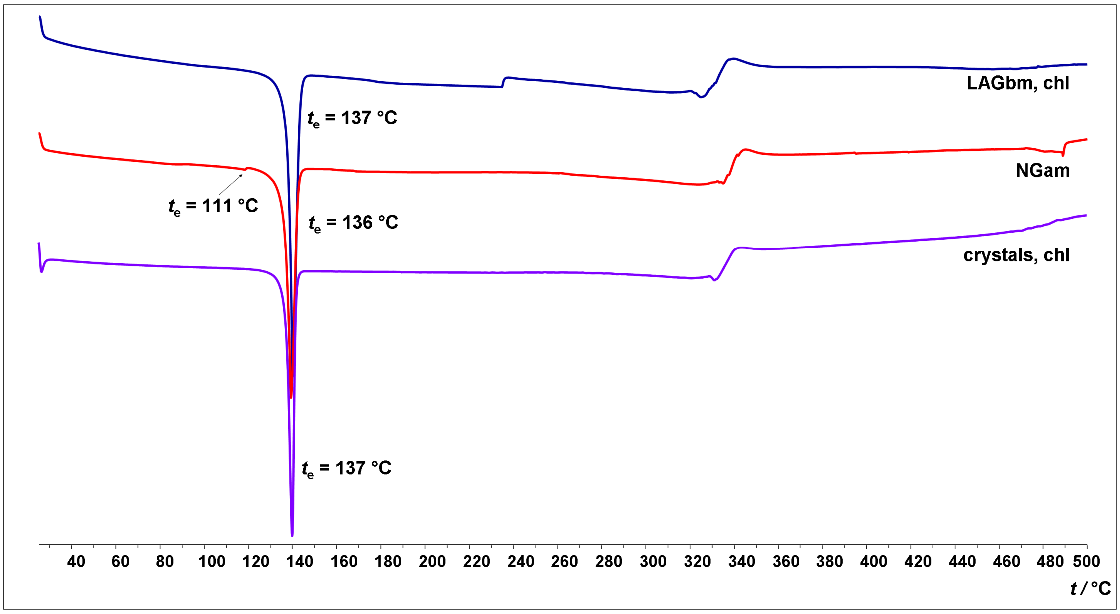

Figure S31. DSC curves for the bulk crystals of **4** obtained by slow evaporation of chloroform, of the product obtained by neat grinding in the mortar (**NGam**) and of the product obtained by chloroform assisted grinding in the ball mill (**LAGbm, chl**).

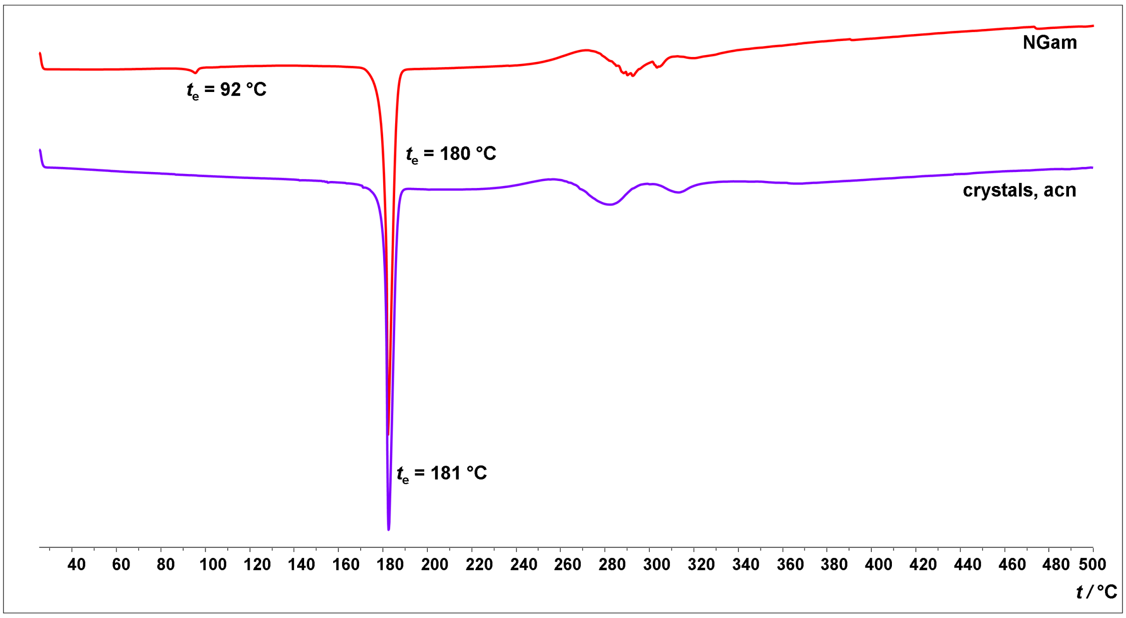

Figure S32. DSC curves for the bulk crystals of **5** obtained by slow evaporation of acetonitrile and of the product obtained by neat grinding in the mortar (**NGam**).

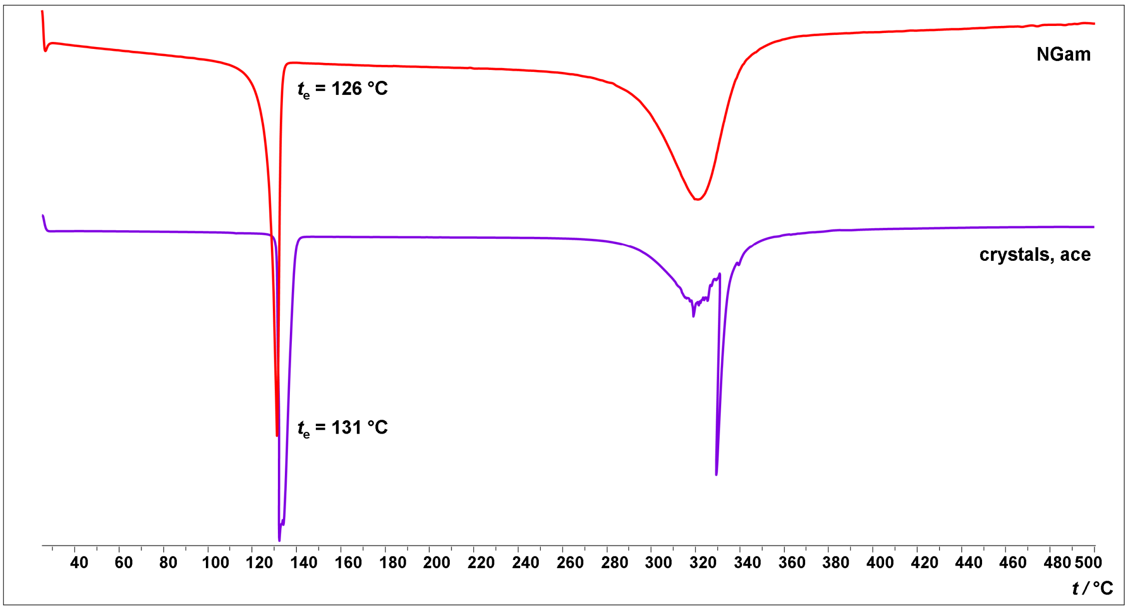

Figure S33. DSC curves for the bulk crystals of **6** obtained by slow evaporation of acetone and of the product obtained by neat grinding in the mortar (**NGam**).

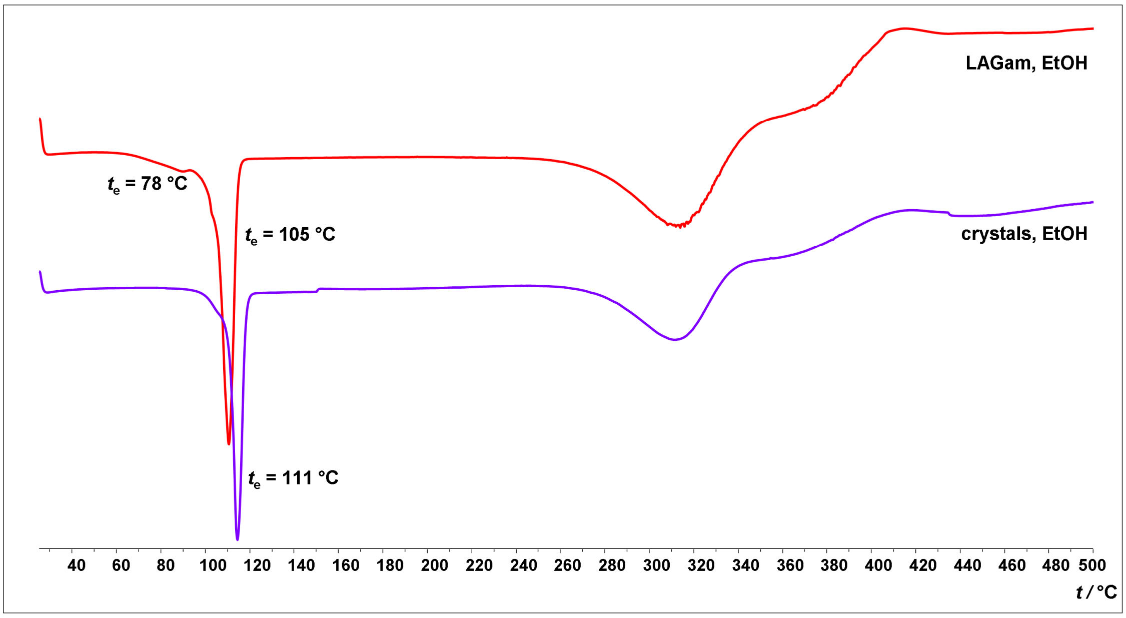

Figure S34. DSC curves for the bulk crystals of **7** obtained by slow evaporation of ethanol and of the product obtained by ethanol assisted grinding in the mortar (L**AGam**).

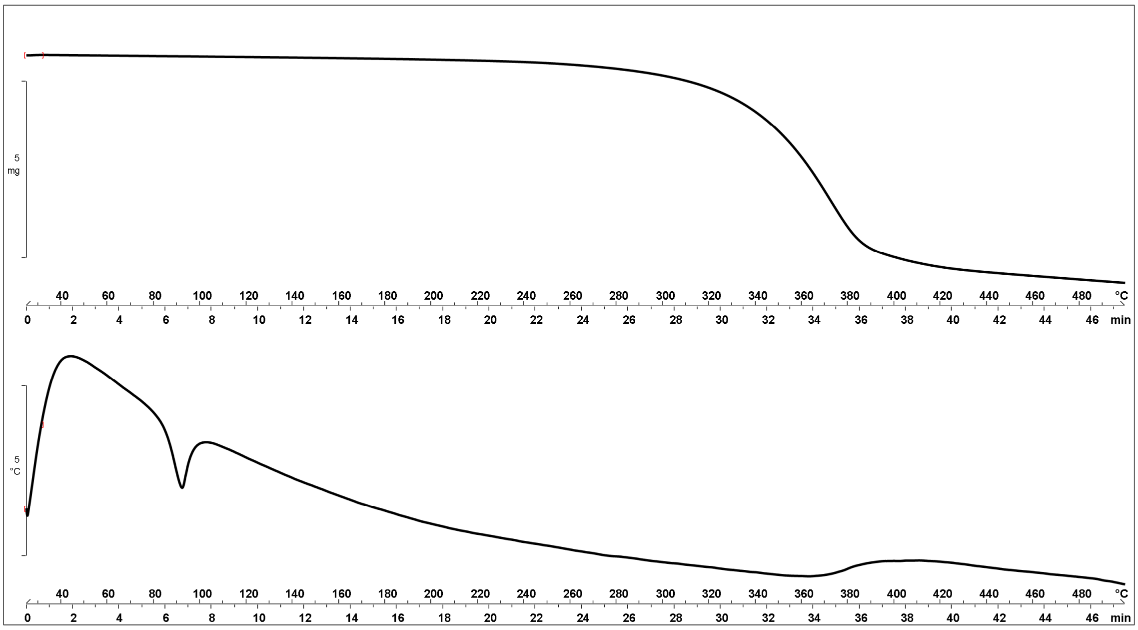

Figure S35. TGA curve for the bulk crystals of **2**.

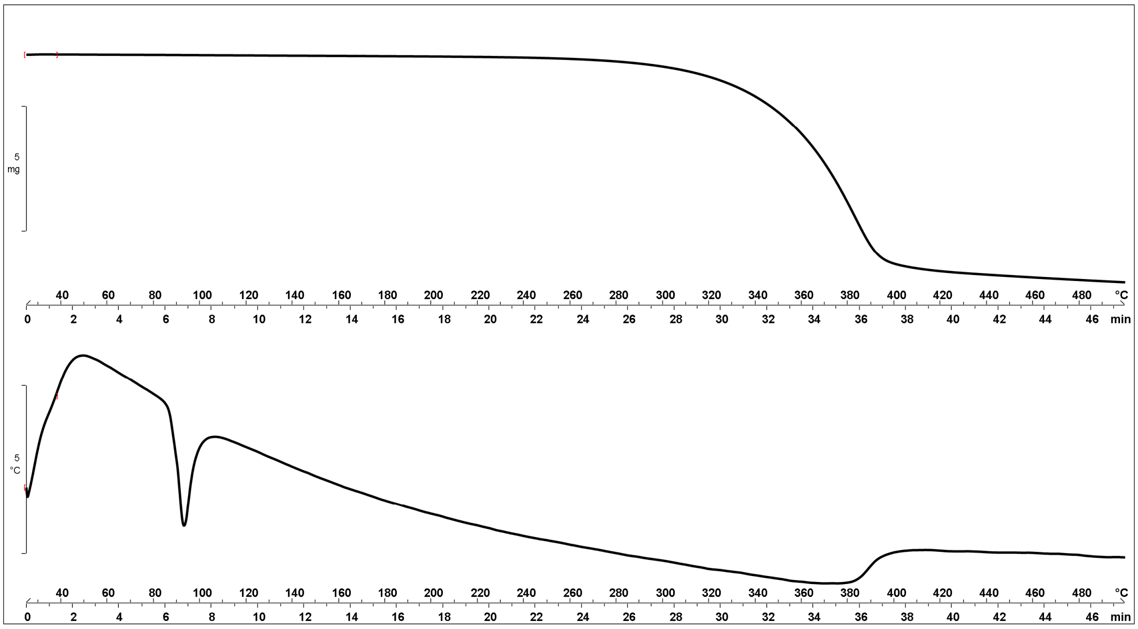

Figure S36. TGA curve for the bulk crystals of **3a**.

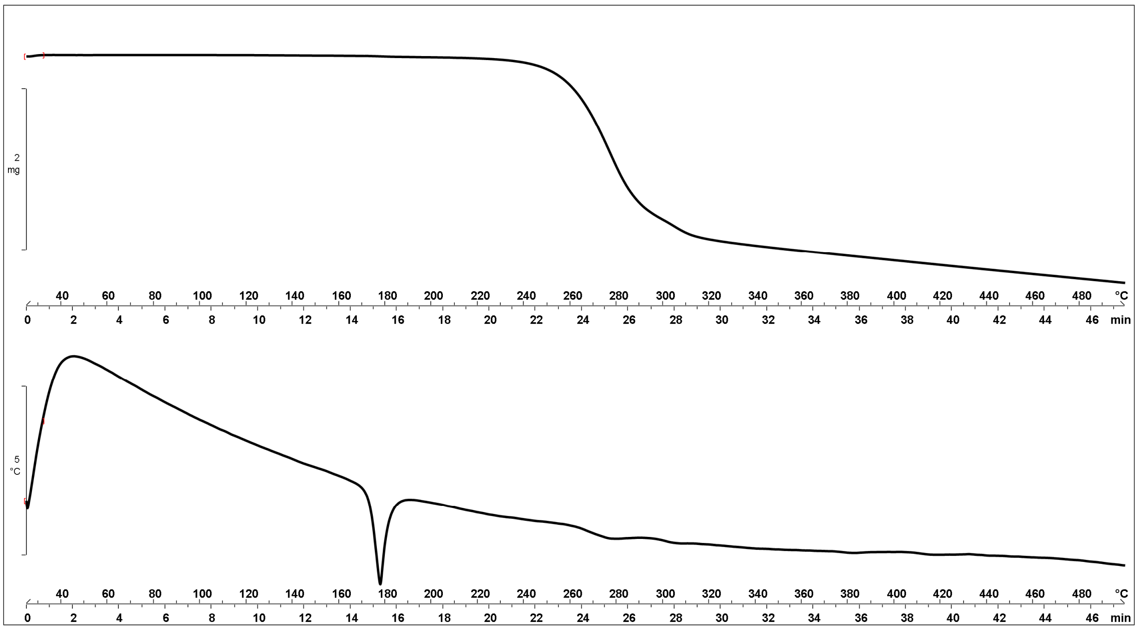

Figure S37. TGA curve for the bulk crystals of **5**.

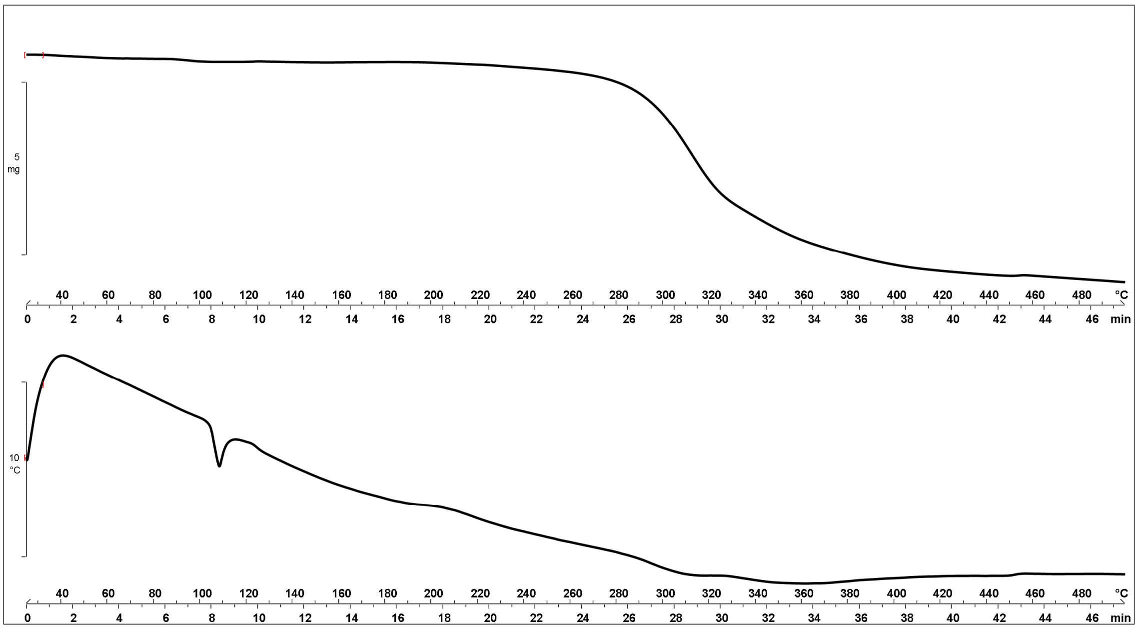

Figure S38. TGA curve for the bulk crystals of **7**.

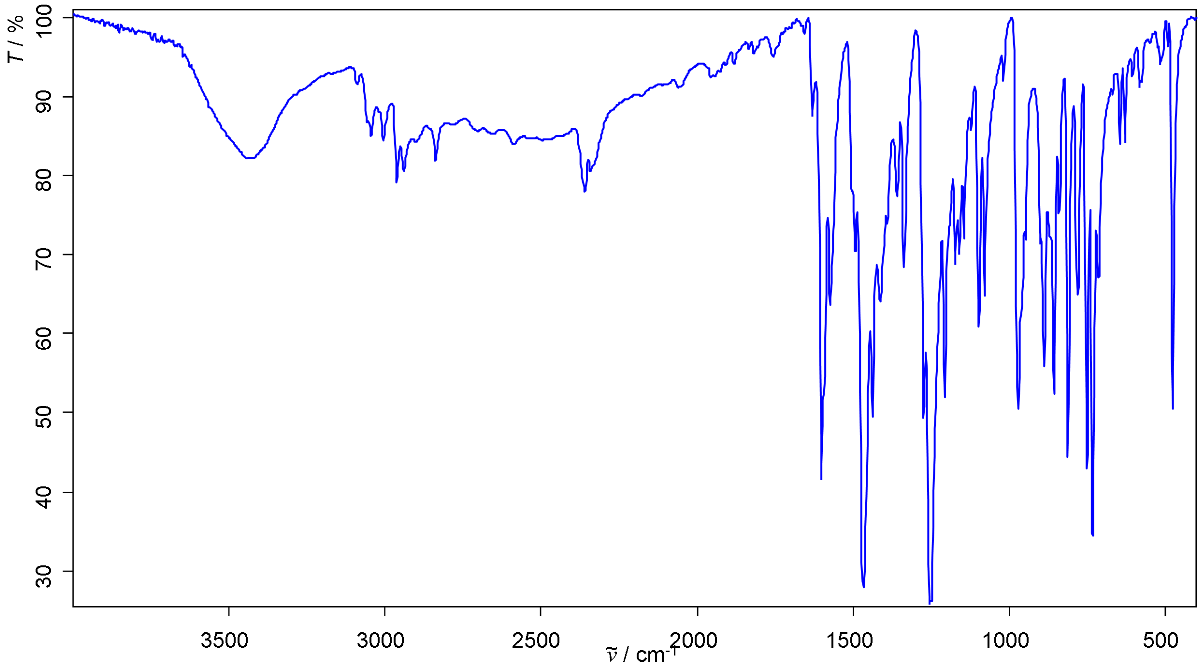

Figure S39. IR spectrum for **2**.

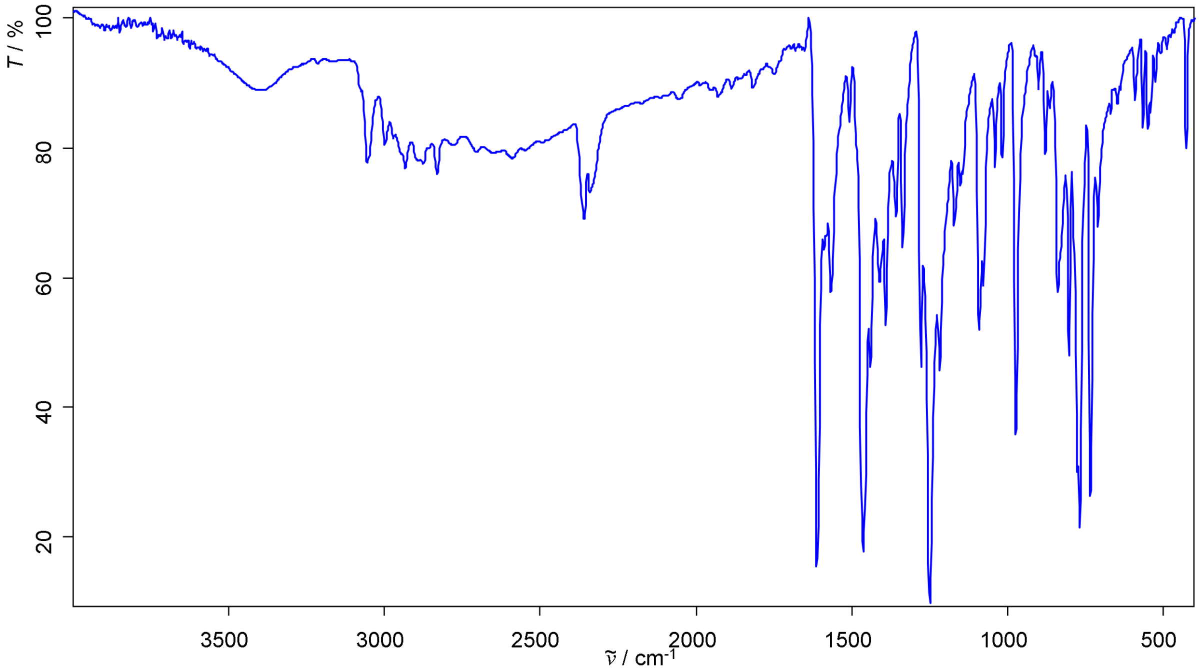

Figure S40. IR spectrum for **3a**.

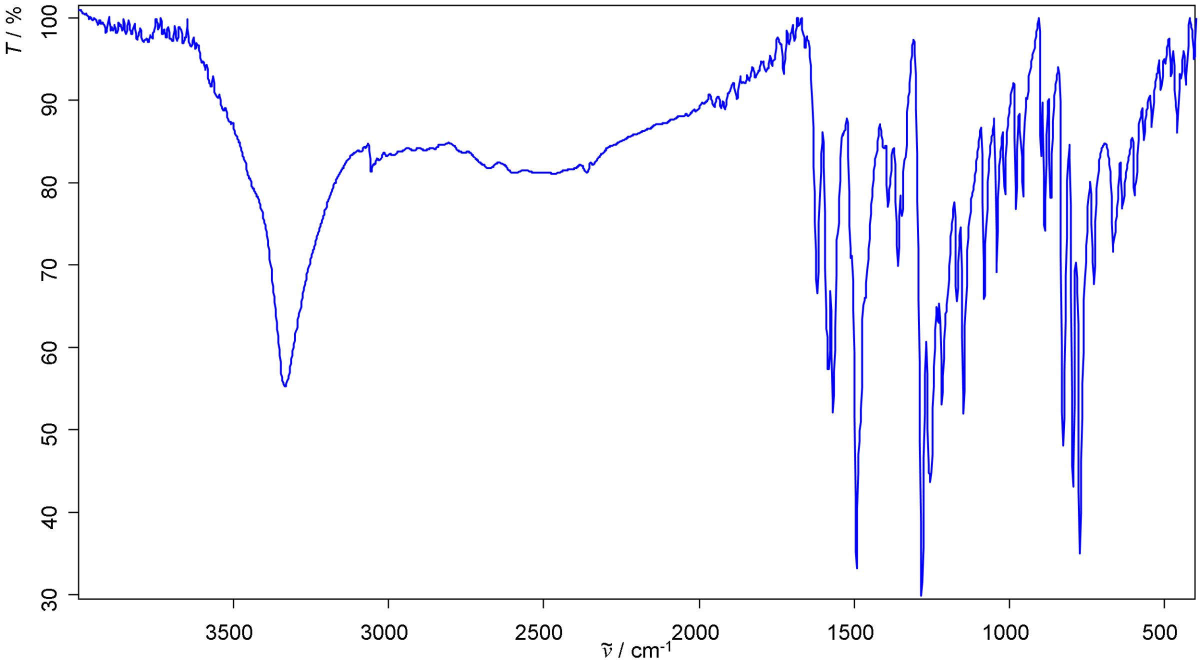

Figure S41. IR spectrum for **5**.

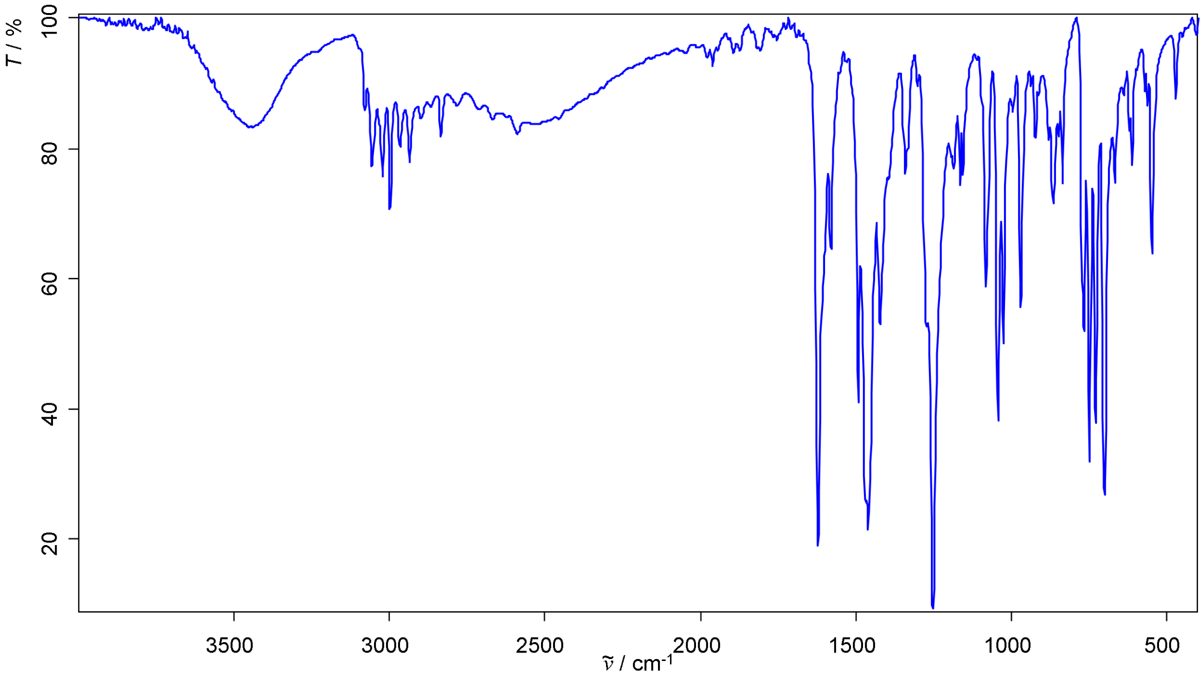

Figure S42. IR spectrum for **7**.

Table S12. Characteristic stretching bands for **2**, **3a**, **5** and **7** found in the FT-IR spectra.

	$\tilde{\nu}$ / cm^{-1}						
	X–H, X = N or O	**C$_{ar}$–H, C–H**	**C=N**	**C$_{ar}$–O**	**C$_{ar}$– C$_{ar}$**	**C$_{ar}$–N**	**C$_{ar}$-O-CH$_3$**
2	3442	3045, 2962	1632	1274 (1467)	1574, 1494	1338	1173
3a	3446	3055, 2831	1612	1249 (1463)	1567, 1508	1336	1169
5	3333	3053	1619	1493 (1282)	1584, 1567	1358	
7	3452	3056, 3022, 2998, 2966	1621	1252 (1460)	1581, 1492	1339	1165

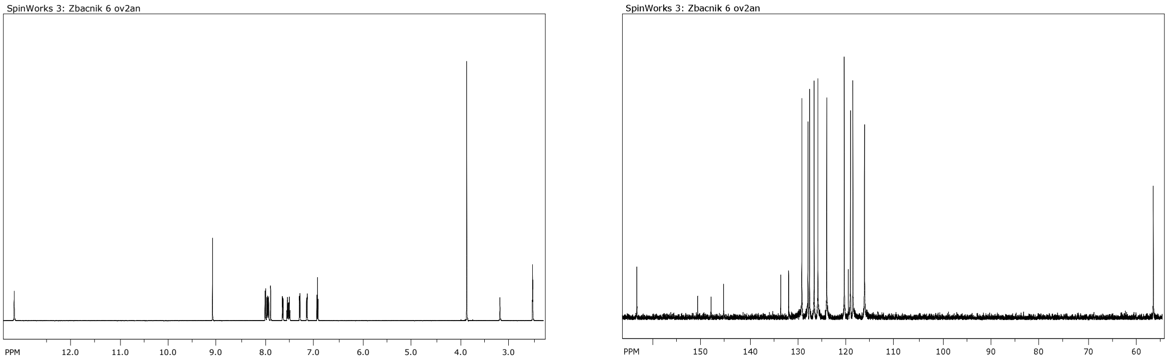

a) b)

Figure S43. a) ^{1}H-NMR and b) ^{13}C-NMR spectrum for **2**.

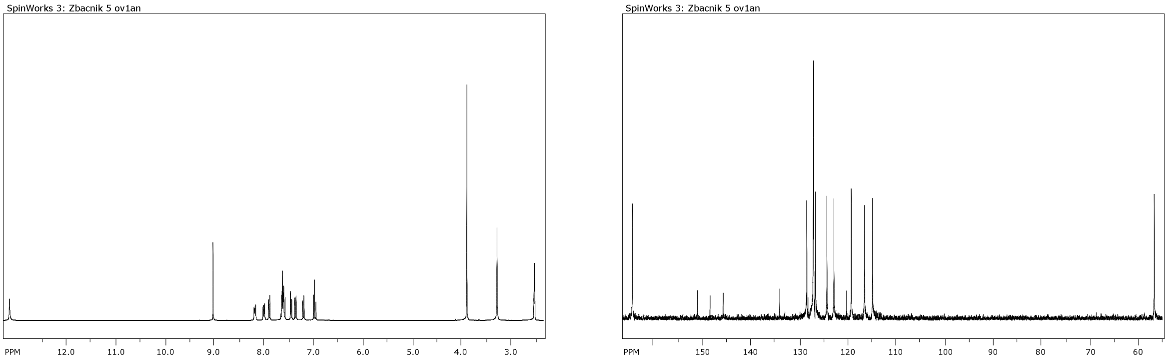

a) b)

Figure S44. a) ^{1}H-NMR and b) ^{13}C-NMR spectrum for **3a**.

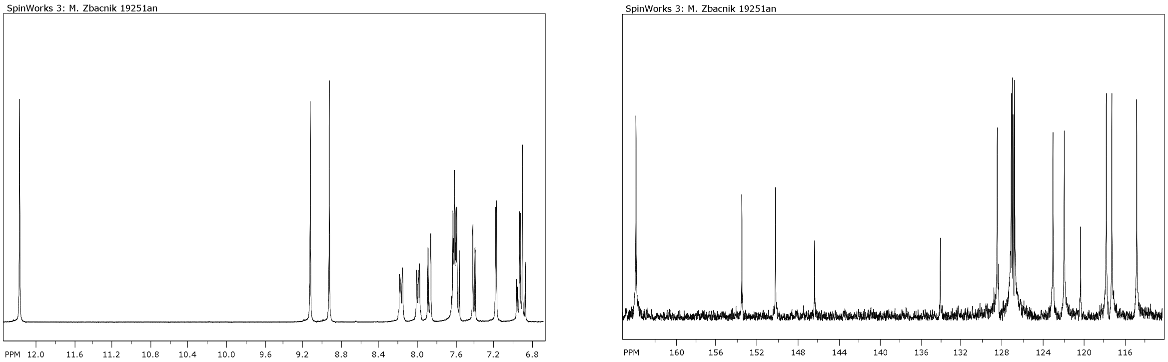

a) b)

Figure S45. a) ^{1}H-NMR and b) ^{13}C-NMR spectrum for **5**.

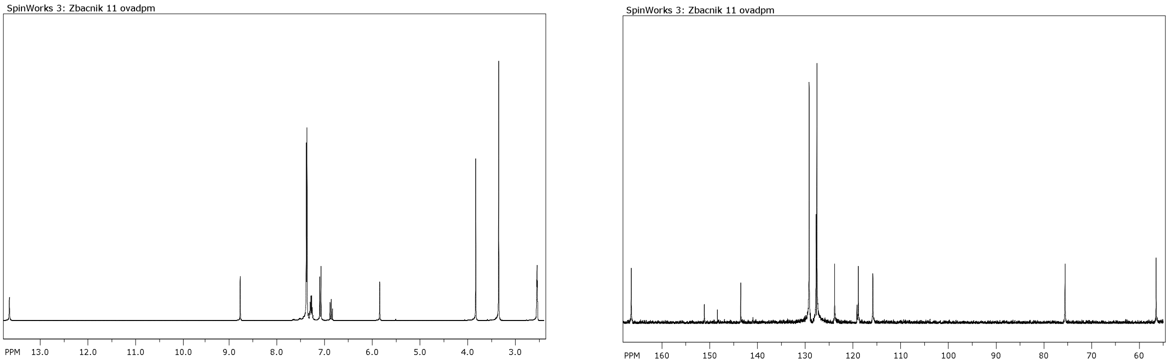

a) b)

Figure S46. a) ^{1}H-NMR and b) ^{13}C-NMR spectrum for **7**.

Table S13. Characteristic signals for **2**, **3a**, **5** and **7** found in the ^{1}H-NMR spectra.

	***δ* / ppm (*J* / Hz)**				
	$H_{aldehyde}$, H_{amine}	**H1 (s)**	**H7 (s)**	**H (s) ($O–CH_3$)**	**other (s)**
2	6.93 t (7.77); 7.15 dd (8.02);7.30 dd (7.88); 7.51 dt (7.38); 7.55 dt (7.38); 7.65 dd (8.66); 7.90 ds; 7.95 d (8.02); 7.97 d (7.93); 8.00 d (8.75)	13.18	9.10	3.86	
3a	6.97 t (7.90); 7.20 dd (8.00); 7.36 dd (7.90); 7.45 dd (7.41); 7.59 d (8.13); 7.62 dd (6.58); 7.63 t (5.25); 7.90 d (8.26); 8.00 t (5.26); 8.19 t (5.25)	13.17	9.04	3.88	
5	6.89 d (8.66); 6.93 dd (8.93); 7.17 ds; 7.40 dd (7.20); 7.60 m 3H; 7.87 d (8.26); 8.00 t (4.95); 8.17 t (4.82)	12.18	8.92		9.12 (O2)
7	6.86 t (7.99); 7.09 d (7.93) 2H; 7.29 m 3H; 7.38 d (4.38) 9H	13.66	8.79	3.81	5.84 (C8)

Table S14. Characteristic signals for **2**, **3a**, **5** and **7** found in the ^{13}C-NMR spectra.

	***δ* / ppm**			
	C2	**C7**	**$C_{aromatic}$**	**other**
2	145.5	163.5	116.2; 119.1; 118.6; 119.5; 120.4; 125.9; 126.6; 127.6; 127.9; 129.2; 132.2; 133.6; 148.1; 150.8	56.2 (C18)
3a	148.6	163.7	114.9; 116.5; 119.3; 120.2; 122.9; 124.3; 126.7; 127.1; 127.1; 127.2; 128.5; 128.5; 134.1; 145.8	56.3 (C18)
5	150.3	164.0	114.8; 117.2; 117.7; 120.3; 121.9; 123.0; 126.8; 126.9; 127.0; 127.1; 128.3; 128.5; 134.1; 146.4; 153.5	
7	148.4	166.5	115.8; 118.8; 119.1; 123.8; 127.5; 127.5; 127.5; 127.5; 127.7; 127.7; 129.2; 129.2; 129.2; 129.2; 143.5; 143.5; 151.1	56.4 (C18)

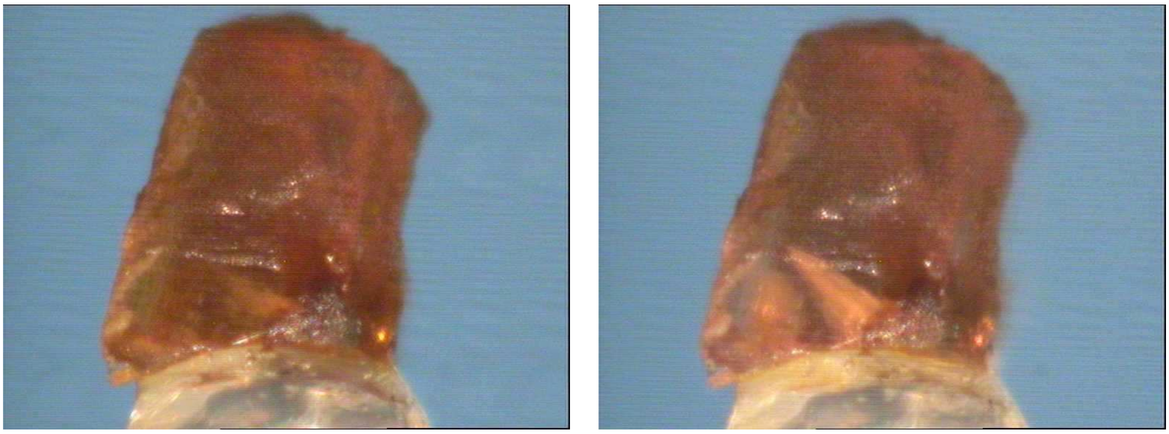

a) b)

Figure S47. Photographs showing solid-state thermochromism of **1** at a) 298 and b) 110 K.

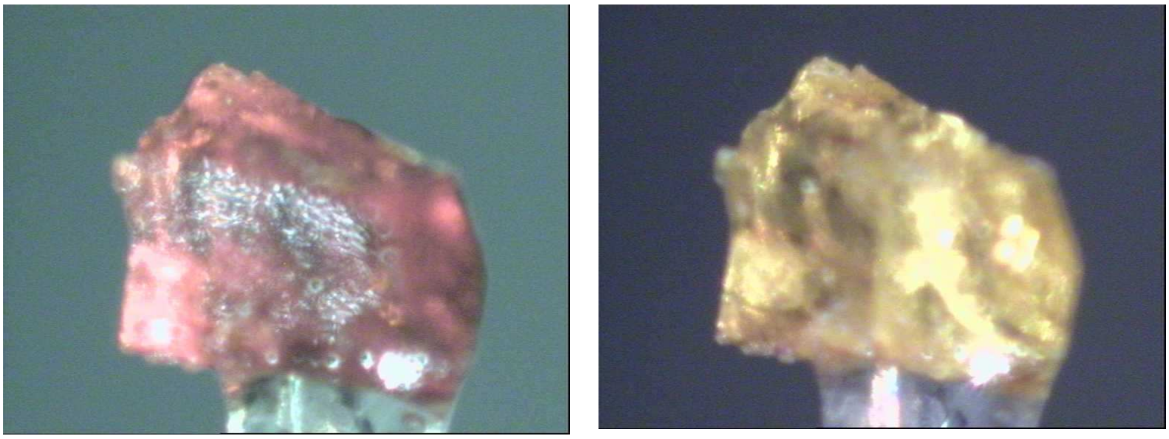

Figure S48. Photographs showing solid-state thermochromism of **2** at a) 298 and b) 110 K.

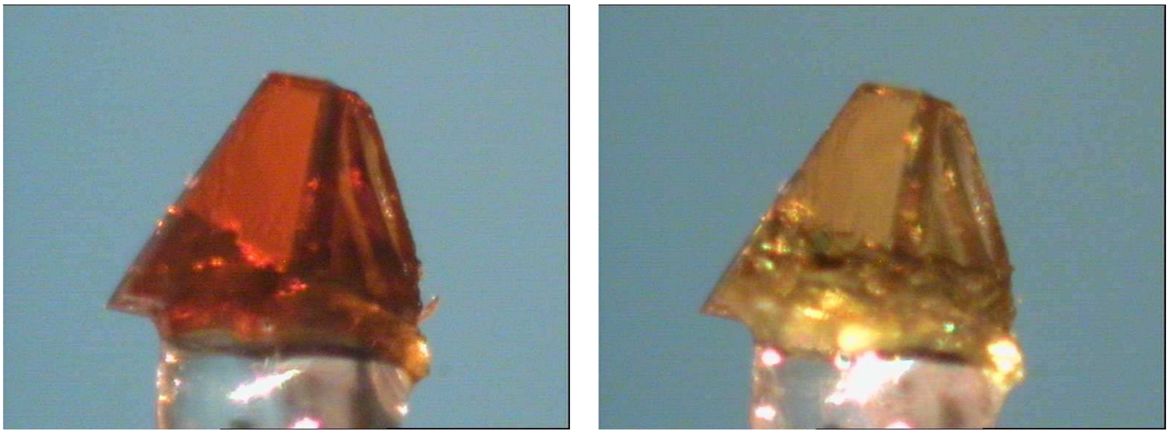

Figure S49. Photographs showing solid-state thermochromism of **3a** at a) 298 and b) 110 K.

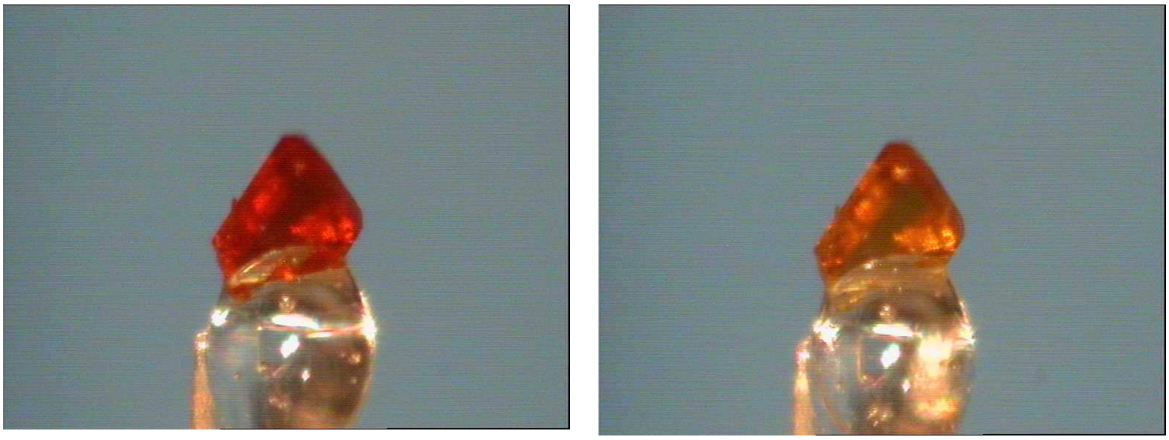

Figure S50. Photographs showing solid-state thermochromism of **3b** at a) 298 and b) 110 K.

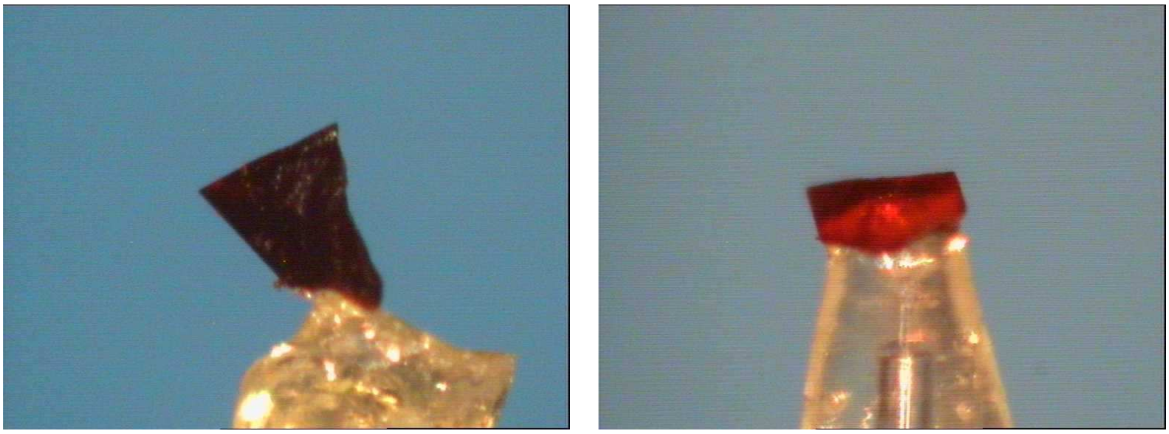

Figure S51. Photographs showing solid-state thermochromism of **4** at a) 298 and b) 110 K.

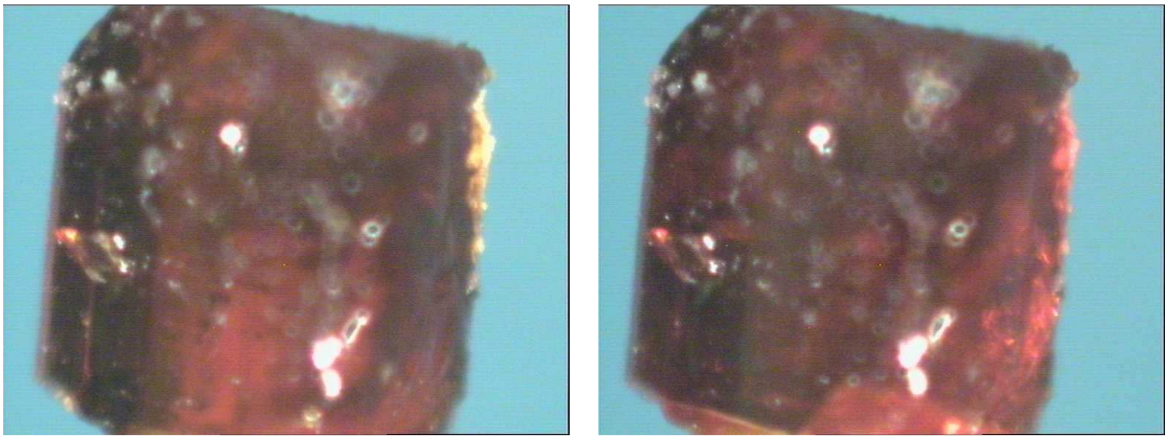

Figure S52. Photographs showing solid-state thermochromism of **5** at a) 298 and b) 110 K.

Figure S53. Photographs showing solid-state thermochromism of **6** at a) 298 and b) 110 K.

Figure S54. Photographs showing solid-state thermochromism of **7** at a) 298 and b) 110 K.

References

---

1 H. M. A. Sharif, D. A. Alvia and S. Yousuf, *Acta Crystallogr.*, 2012, **E68**, o2629.
2 H. Ünver, M. Yıldız, B. Dülger, Ö. Özgen, E. Kendi and T. N. Durlu, *J. Mol. Struct*., 2005, **737**, 159.
3 Özek, S. Yüce, C. Albayrak, M. Odabasoglu and O. Büyükgüngör, *Acta Crystallogr.*, 2005, **E61**, o3179.
4 Y. Xiu-Guang, Z. Lu-Ping, H. Yun-Ling and Z. Zheng-Da, *Z. Kristallogr.-New Cryst. Struct*., 2012, **227**, 249.
5 STAR^e Software V.9.01., MettlerToledo GmbH, 2006.
6 OPUS 4.0, Brucker Optik GmbH, 2003.
7 K. Marat, SpinWorks 3, Version 3.1.0.0., 2009, http://home.cc.umanitoba.ca/wolowiec/spinworks/index.html
8 Oxford Diffraction (2003), *CrysAlis CCD and CrysAlis RED*. Version 1.170., Oxford Diffraction Ltd, Wroclaw, Poland.
9 G. M. Sheldrick, *Acta Crystallogr*., 2008, **A64**, 112.
10 L. J. Farrugia, WinGX, *J. Appl. Cryst.*, 1999, **32**, 837.
11 Crystallographic data have been deposited with the Cambridge Crystallographic Data Centre, 12 Union Road, Cambridge, CB2 1EZ, UK (fax: +44 1223 336033; e-mail: deposit@ccdc.ac.uk or www: http://www.ccdc.cam.ac.uk). These data can be obtained free of charge from the Director upon request quoting the CCDC deposition numbers 973331–973338.
12 L. J. Farrugia, ORTEP-3 for Windows, *J. Appl. Cryst.*, 1997, **30**, 565.
13 C. F. Macrae, I. J. Bruno, J. A. Chisholm, P. R. Edgington, P. McCabe, E. Pidcock, L. Rodriguez-Monge, R. Taylor, J.v.d. Streek and P. A. Wood, *J. Appl. Crystallogr.,* 2008, **41**, 466.
14 *Philips X'Pert Data Collector 1.3e*, Philips Analytical B. V. Netherlands, 2001**.**
15 *Philips X'Pert Graphic & Identify 1.3e* Philips Analytical B. V. Netherlands, 2001**.**
16 *Philips X'Pert Plus 1.0,* Philips Analytical B. V. Netherlands, 1999**.**